Progress in Oceanography 182 (2020) 102272

Contents lists available at ScienceDirect

Progress in Oceanography

journal homepage: www.elsevier.com/locate/pocean

Partial pressure of CO_2 and air-sea CO_2 fluxes in the South China Sea: Synthesis of an 18-year dataset

Qian Li[a,1], Xianghui Guo[a,b,*], Weidong Zhai[c], Yi Xu[a], Minhan Dai[a,b]

[a] State Key Laboratory of Marine Environmental Science, Xiamen University, Xiamen 361102, China
[b] College of Ocean and Earth Sciences, Xiamen University, Xiamen 361102, China
[c] Institute of Marine Science and Technology, Shandong University, Qingdao 266237, China

ARTICLE INFO

Keywords:
South China Sea (SCS)
Partial pressure of CO_2
Air-sea CO_2 fluxes
Marginal Sea
Intra-seasonal variability
Seasonal variability

ABSTRACT

This study synthesizes spatial and temporal variations in surface seawater pCO_2 (partial pressure of CO_2) and associated air-sea CO_2 fluxes in the largest marginal sea of the North Pacific, the South China Sea (SCS), based on a large dataset collected from 47 surveys during 2000–2018. We categorized the SCS into five domains featuring different physical and biogeochemical characteristics to better understand the seasonality of SCS pCO_2 dynamics and constrain the CO_2 fluxes. The five domains are (A) the northern SCS shelf, (B) the northern SCS slope, (C) the SCS basin, (D) West of the Luzon Strait, and (E) the western SCS. We found a large spatial variability in sea surface pCO_2 in the SCS, except during winter when values remained in a narrow range of 300 to 360 μatm. In general, seasonal variability was evident in surface water pCO_2 values from the northern SCS (Domains A, B and D), with lower values during the cold seasons and higher values during the warm seasons, except in the Pearl River plume (150–650 μatm) and the area off northwest Luzon where winter upwelling occurred (370–470 μatm). In the SCS basin and the western SCS (Domains C and E), pCO_2 in surface waters was generally higher than in the atmosphere (380–420 μatm). We also revealed large intra-seasonal variations in the northern SCS during monsoonal transitions in both spring and fall. In spring, pCO_2 increased with temperature in the northern SCS, which was a CO_2 sink in March but became a CO_2 source in May with April as a transitional month. Fall is also a transitional season for the northern SCS, where it changes from a CO_2 source back to a CO_2 sink. The area-weighted CO_2 fluxes across the entire SCS were -1.1 ± 2.2 mmol m^{-2} d^{-1} in winter, 0.9 ± 0.9 mmol m^{-2} d^{-1} in spring, 2.5 ± 1.4 mmol m^{-2} d^{-1} in summer and 1.9 ± 1.1 mmol m^{-2} d^{-1} in fall. Nevertheless, on an annual basis, the average CO_2 flux from the SCS was 1.2 ± 1.7 mmol m^{-2} d^{-1}. Enhanced carbon sink on the northern SCS shelf was observed in winter. The annual average CO_2 flux was significantly lower than the previous estimate, which can largely be attributed to the addition of new datasets in the previously under-sampled seasons and regions.

1. Introduction

Air-sea CO_2 fluxes in marginal seas serve as an important component of the ocean's carbon cycle (Jiang et al., 2008, Laruelle et al., 2018, Marrec et al., 2015, Thomas and Schneider, 1999). With the rapid growth of CO_2 flux measurements during the past decades, our estimations of marginal sea air-sea CO_2 fluxes have converged to about 0.2 to 0.5 Pg C yr^{-1} at the global scale (Borges et al., 2005, Cai et al., 2006, Chen and Borges, 2009, Chen et al., 2013, Dai et al., 2013, Laruelle et al., 2010, Laruelle et al., 2014). It remains challenging however to reliably assess the carbon fluxes in individual coastal systems, which often feature large spatial and temporal variations and are often complicated by the influences of mesoscale processes such as river plumes (Huang et al., 2015), coastal upwelling (Hales et al., 2005) and eddies (Zhou et al., 2013), as well as dynamic cross-shelf and/or shelf-ocean exchanges (Wang et al., 2013). These processes are often associated with strong biological and chemical responses, leading to complex spatial and seasonal overprinting on CO_2 fluxes. Additionally, seasonal asymmetry due to changes in temperature and biophysical drivers adds more complexity to the marine CO_2 system (Fassbender et al., 2018, Woosley, 2018), requiring higher temporal resolution of observations down to at least intra-seasonal scales. Moreover, marginal seas are subject to both remote forcings, such as ENSO (Chao et al., 1996, Ma et al., 2016), and localized drivers, such as river plumes and

* Corresponding author.
E-mail address: xhguo@xmu.edu.cn (X. Guo).
[1] Now at School of Marine Science and Policy, University of Delaware, Newark, DE 19716, USA.

https://doi.org/10.1016/j.pocean.2020.102272

Available online 20 January 2020

Table 1
Summary of the five physico-biogeochemical domains categorized in the South China Sea.

Domain	Location	Longitude (°E)	Latitude (°N)	Surface area (10^5 km^2)	Description and characteristics
A	NSCS shelf	109.5–119.0	16.9–24.0	2.4848	Shallower than 200 m; influenced by the Pearl River plume, coastal upwelling and coastal currents; high Chl-a in all seasons
B	NSCS slope	109.5–118.0	16.9–21.95	1.4077	Area linking the northern shelf with the oligotrophic basin and the western slope; relatively higher Chl-a in winter than in other seasons
C	SCS basin	114–119.3	10.8–20.2	4.3101	Generally deeper than 3000 m excluding the zones influenced by the winter upwelling near Luzon Strait and the eddies off Vietnam; generally characterized by low Chl-a in all seasons
D	West of Luzon Strait	118–120.5	18–23	1.3132	Influenced by the Kuroshio and winter upwelling; characterized by higher Chl-a in winter
E	WSCS slope and basin	109.5–114	10–18	4.0261	Influenced by the Mekong River plume and cyclonic eddies, with high Chl-a in summer and early fall

coastal upwelling (Friederich et al., 2002, Huang et al., 2015). Since time-series observations are often lacking in the world's marginal seas, we have only begun to understand inter-annual variations in their carbon cycles (Salt et al., 2013, Wesslander et al., 2010).

The South China Sea (SCS) is a large marginal sea system experiencing multiple scales of physical and biogeochemical modulations. It is also one of the most studied marginal seas in the world; field observation-based studies of air-sea CO_2 fluxes began in the 1990s and early 2000s (Chen et al., 2006, Chou et al., 2005, Rehder and Suess, 2001, Zhai et al., 2005). According to Chou et al. (2005), the northern SCS (NSCS) acts as a CO_2 sink with an annual CO_2 flux of -0.30 to -0.63 mmol m^{-2} d^{-1} based on observations at the South East Asia Time-series Study (SEATS) station (116 °E, 18 °N) from March 2002 to April 2003. Based on data collected from September 1999 to October 2003 at the same station, Tseng et al. (2007) stated that the NSCS basin is a very weak sink of atmospheric CO_2 of 0.05 mmol m^{-2} d^{-1}. However, Sheu et al. (2010) reported that the NSCS basin acts as a weak CO_2 source based on the longer observation period of 1999–2008 at the SEATS station, with an annual average CO_2 flux of 0.60–0.64 mmol m^{-2} d^{-1}. Sheu et al. (2010) also observed the influence of ENSO, with air-sea CO_2 fluxes 85% lower during El Niño than La Niña periods. Based on measurements of the partial pressure of CO_2 (pCO_2) in the area of the NSCS shelf and slope, Zhai et al. (2005) suggested that the NSCS is a CO_2 source of 1–7 mmol m^{-2} d^{-1} from spring to fall, with sea surface temperature (SST) dominating the seasonal variations in surface water pCO_2. In the SCS basin, Chen et al. (2006) suggested that the relatively high temperature seasons/areas act as a CO_2 source while the relatively low temperature seasons/areas act as a CO_2 sink, and also that surface water pCO_2 is controlled primarily by SST. Based on cruise data, Chen et al. (2006) calculated that the entire SCS basin acts as a CO_2 source of 0.7 mmol m^{-2} d^{-1} during warm seasons and a CO_2 sink of 0.5 mmol m^{-2} d^{-1} during cold seasons. Xu et al. (2016) showed that the western SCS (WSCS) is a CO_2 source of 0.9–2.9 mmol m^{-2} d^{-1} in fall, and that surface water pCO_2 is primarily controlled by SST with significant influences from the Mekong River plume and coral reefs on pCO_2 distributions. The Borneo-Palawan-Luzon coast in early fall (September) is a CO_2 source of 0.3–2.6 mmol m^{-2} d^{-1} (Rehder and Suess, 2001).

Based on data collected from 14 field surveys in the SCS, Zhai et al. (2013) subdivided the SCS into four physico-biological domains and estimated that the SCS acts as a CO_2 source of 3.1 ± 2.3 mmol m^{-2} d^{-1}, which is similar to the average flux from the tropical ocean. Events such as typhoons, upwelling and cold-core eddies have a significant influence on the air-sea CO_2 fluxes, and may change sink-source patterns (Xu et al., 2016, Zhai et al., 2013). However, intra-seasonal variability is still unresolved. Additionally, the CO_2 fluxes in some areas are based on only one survey, and the influences of such events may result in biased flux estimates when extrapolated over a longer period of time.

In this study, we integrated new data collected in the SCS from 2009 to 2018 with the data collected from 2000 to 2008 (Zhai et al., 2013, Zhai et al., 2009, Zhai et al., 2005). We aim to reveal (1) intra-seasonal variability of the CO_2 sinks/sources; (2) the seasonal and spatial variations of surface water pCO_2 and air-sea CO_2 fluxes; (3) the potential interannual variations in CO_2 fluxes; and (4) the major flux controls in each physically and biogeochemically distinct regions of the SCS.

In order to better answer the above questions, we categorized the SCS into five domains with distinct physico-biogeochemical characteristics. Further to Zhai et al. (2013), our categorization of the domains is based on both topography and chlorophyll-a (Chl-a) distributions. Domain A is the dynamic NSCS shelf region shallower than 200 m, which is characterized by relatively high Chl-a throughout the year. Domain B is the NSCS slope (200–3000 m), linking the shelf and the oligotrophic basin. Domain B is characterized by relatively high Chl-a in fall and winter, but low Chl-a in spring and summer. Domain C is the oligotrophic SCS basin, which is generally deeper than 3000 m and

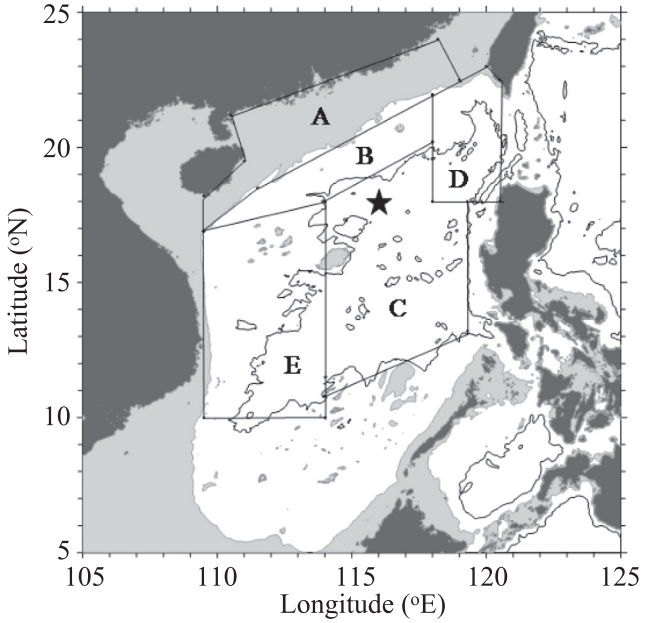

Fig. 1. Map of the South China Sea. The grey areas are shallower than 200 m and the black contour is the 3000 m isobath. The five physico-biogeochemical domains are also shown. The star shows the location of the SEATS station.

characterized by low Chl-a throughout year, excluding the zone influenced by winter upwelling off Luzon Island and the eddies off Vietnam. Domain D is the area west of the Luzon Strait, which is characterized by high Chl-a in winter as a result of winter upwelling. Domain E is the area influenced by the Mekong River plume and eddies and characterized by relatively high Chl-a in summer and fall. The boundaries, surface areas and characteristics of the five domains are presented in Table 1 and Fig. 1. Distributions of Chl-a are shown in Supplementary materials (Fig. S1).

2. Study areas

The SCS is located in the northwestern Pacific Ocean, extending from 23°N in the sub-tropics at southern Taiwan to 3°S in the tropics at the coasts of Borneo and Sumatra, with a surface area of 3.6×10^6 km^2 (Chen et al., 2001). The SCS is a semi-closed marginal sea, connecting to the East China Sea through Taiwan Strait, to the western North Pacific through the Luzon Strait, to the Sulu Sea through the Mindoro Strait, and to the Java Sea through the Karimata Strait. Among the straits, the Luzon Strait is the only deep channel (2200 m) connecting the SCS to the Pacific. The Kuroshio current, characterized by high salinity and temperature, has influence on the SCS by intrusion through the Luzon Strait (Caruso et al., 2006).

The central and northeastern SCS is an oligotrophic basin with a maximum depth of > 5000 m. In the northeast of the basin off Luzon Island, episodic strong winter upwelling induces CO_2 evasion to the atmosphere (Zhai et al., 2013). The northern boundary of the basin is the broad NSCS shelf. The Gulf of Thailand and Sunda Shelf make up the southwestern and southern shelf portion of the SCS shallower than 50 m (Chen et al., 2001). The Pearl River and Mekong River discharge into the NSCS and the WSCS, respectively, with respectively annual runoffs of 3.3 and 4.7×10^{11} m^3 (Dai et al., 2014, McKee et al., 2004). The SCS is located in the tropical and subtropical monsoon regime. Under the influence of the monsoon, the general surface circulation in the SCS is cyclonic in winter but anti-cyclonic in summer (Hu et al., 2000, Liu et al., 2008, Su, 2004). Thus, the western boundary of the SCS is very dynamic. Consistent with these large scale circulation patterns, the coastal current moves southwestwardly in winter and northeastwardly in summer (Hu et al., 2000). In summer, high discharge from the large rivers forms plumes on the NSCS shelf (Gan et al., 2009) and in the WSCS off Vietnam (Chen et al., 2010). Under the influence of the summer monsoon, coastal upwelling is also prevalent in the NSCS and WSCS (Dippner et al., 2007, Gan et al., 2009). In the WSCS off Vietnam, the strong eastward baroclinic jet in summer frequently generate eddies (Wang et al., 2003). Multiple influences including the river plumes, coastal upwelling and eddies adds to the complexity of the coastal physical dynamics and biogeochemical processes. Typhoons in the SCS are also active from spring to fall, especially in summer (Guan et al., 2011, Tang et al., 2011).

Generally, the NSCS has high SSTs in summer and early fall but low SSTs in winter and early spring. In summer, river inputs and coastal upwelling stimulate primary production on the NSCS shelf (Cao et al., 2011, Tan and Shi, 2009). However, the NSCS slope and basin are generally oligotrophic and characterized by low productivity (Chen, 2005). In winter, the mixed layer deepens and productivity increases (Chen, 2005). In the area of the WSCS shelf and slope, the Mekong River plume and eddies promote primary production in summer and early fall (Tan and Shi, 2009).

3. Materials and methods

3.1. Measurements of pCO_2, SST, SSS and auxiliary parameters

47 cruises/legs were conducted from 2000 to 2018 in the SCS onboard the R/Vs Dongfanghong 2, Yanping 2, Shiyan 3, Jiageng (TKK), Haijian 83, Haidiao 6 and Kexue 3. Survey periods and related information are listed in Table 2. Cruise tracks are shown in Fig. 2. During the cruises, SST, sea surface salinity (SSS) and pCO_2 were measured continuously. The measurement and data processing methods followed those of Pierrot et al. (2009) and the SOCAT (Surface Ocean CO_2 Atlas, http://www.socat.info/news.html) protocol, which are briefly summarized here.

pCO_2 was measured continuously with a non-dispersive infrared spectrometer (Li-Cor® 7000) or by Cavity Ring-Down Spectroscopy (Picarro G2301) integrated in a GO-8050 system (General Oceanic Inc. USA) onboard the Dongfanghong 2 and Haidiao 6, or with a homemade continuous measurement system onboard the other research vessels. The GO-8050 system is described by Pierrot et al. (2009). The homemade system is described by Zhai et al. (2005), Zhai et al. (2009) and Zhai et al. (2013). Surface water was continuously pumped from ~3–5 m depth and CO_2 mole fraction (xCO_2) was determined after air–water equilibration. xCO_2 in the atmosphere was determined every ~1–1.5 h. The intake for atmospheric air samples was installed at the bow ~10 m above the sea surface to avoid contamination from the ship. The barometric pressure was measured continuously onboard with a barometer fixed ~10 m above the sea surface.

Satellite-derived (from 2003 to 2016) monthly mean SSTs were calculated based on monthly mean SST values obtained from the NASA ocean color website (http://oceancolor.gsfc.nasa.gov), which were retrieved with the Moderate Resolution Imaging Spectroradiometer (MODIS) onboard the Aqua satellite. The 4 μm nighttime SST products were used here.

3.2. Data processing

Water pCO_2 at the temperature in the equilibrator (pCO_2^{Eq}) was calculated from the xCO_2 in dry air in the equilibrator and the pressure in the equilibrator (P_{Eq}) after correcting for the vapor pressure (P_{H2O}) of water at 100% relative humidity (Weiss and Price, 1980):

$$pCO_2^{Eq} = (P_{Eq} - P_{H2O}) \times xCO_2 \quad (1)$$

pCO_2 in the air was calculated similarly using xCO_2 in the air and the barometric pressure, using a formula similar to Formula (1). xCO_2 in the atmosphere over Guam (13.3860°N, 144.6560°E, http://www.esrl.

Table 2
Summary of cruise information (47 total).

Season	Survey period	Surveyed area	R/V	Sampler configuration	Data source
Winter	Dec. 1–23, 2006	A,B,D,E	Dongfanghong 2	Modified from Jiang et al. (2008)	(Zhai et al., 2013)
	Dec. 29–31, 2008	A	Dongfanghong 2	GO-8050	This study
	Jan. 1–11, 2009	A,B	Dongfanghong 2	GO-8050	This study
	Jan. 5–31, 2010	A,B,D	Dongfanghong 2	GO-8050	This study
	Jan. 4–31, 2018	A,B,C,D	Jiageng (TKK)	Modified from Jiang et al. (2008)	This study
	Feb. 10–29, 2004	A,B	Yanping 2	Modified from Zhai et al. (2005)	(Zhai et al., 2013)
	Feb. 15–20, 2006	A,B	Haijian 83	Modified from Zhai et al. (2005)	(Zhai et al., 2013)
	Feb. 1–4, 2018	A	Jiageng (TKK)	Modified from Jiang et al. (2008)	This study
Spring	Mar. 1–5, 2004	A	Yanping 2	Modified from Zhai et al. (2005)	(Zhai et al., 2013)
	Mar. 20–31, 2009	A,D	Dongfanghong 2	GO-8050	(Zhai, 2015)
	Apr. 29, 2004	E	Shiyan 3	Modified from Zhai et al. (2005)	(Zhai et al., 2013)
	Apr. 10–25, 2005	A,C,E	Dongfanghong 2	Modified from Zhai et al. (2005)	(Zhai et al., 2013)
	Apr. 20–30, 2008	D	Dongfanghong 2	GO-8050	(Zhai et al., 2013)
	Apr. 1–21, 2009	A,B,D	Dongfanghong 2	GO-8050	(Zhai, 2015)
	Apr. 9–29, 2012	C	Dongfanghong 2	GO-8050	This study
	May 14–30, 2001	A	Yanping 2	Zhai et al. (2005)	(Zhai et al., 2005)
	May 1–28, 2004	C,E	Shiyan 3	Modified from Zhai et al. (2005)	(Zhai et al., 2013)
	May 1–29, 2011	A,B,C,D	Dongfanghong 2	GO-8050	This study
	May 23–31, 2014	D	Dongfanghong 2	GO-8050	This study
	May 15–31, 2016	A,B	Dongfanghong 2	Modified from Jiang et al. (2008)	This study
Summer	Jun. 2–3, 2001	A	Yanping 2	Zhai et al. (2005)	(Zhai et al., 2005)
	Jun. 1–20, 2014	A,B,C,D	Dongfanghong 2	GO-8050	This study
	Jun. 1–5, 2016	A,B	Dongfanghong 2	Modified from Jiang et al. (2008)	This study
	Jun. 5–27, 2017	A,B,C,E	Jiageng (TKK)	Modified from Jiang et al. (2008)	This study
	Jul. 10–21, 2000	A	Yanping 2	Zhai et al. (2005)	(Zhai et al., 2005)
	Jul 6–23, 2004	A,B,C	Yanping 2	Modified from Zhai et al. (2005)	(Zhai et al., 2013, Zhai et al., 2009)
	Jul. 1–24, 2007	A,B,D	Dongfanghong 2	Modified from Jiang et al. (2008)	(Zhai et al., 2013)
	Jul. 1–14, 2008	A,B,D	Shiyan 3	Modified from Jiang et al. (2008)	This study
	Jul. 17–31, 2009	A,B,D	Dongfanghong 2	GO-8050	This study*
	Jul. 29–31, 2012	A	Dongfanghong 2	GO-8050	This study
	Jul. 1–18, 2014	A,B,C,D	Dongfanghong 2	GO-8050	This study
	Jul. 19–31, 2015	A	Haidiao 6	GO-8050	This study
	Aug. 14–31, 2007	E	Dongfanghong 2	Modified from Jiang et al. (2008)	(Zhai et al., 2013)
	Aug. 6–31, 2008	D	Dongfanghong 2	GO-8050	This study
	Aug. 1–18, 2009	A,B,C,D	Dongfanghong 2	GO-8050	This study#
	Aug. 1–21, 2012	A,B	Dongfanghong 2	GO-8050	This study
	Aug. 1–8, 2015	A	Haidiao 6	GO-8050	This study
Fall	Sep. 18–30, 2004	A,B,D	Shiyan 3	Modified from Zhai et al. (2005)	(Zhai et al., 2013)
	Sep. 30, 2006	A	Kexue 3	Modified from Jiang et al. (2008)	(Zhai et al., 2013)
	Sep. 1–14, 2007	C,E	Dongfanghong 2	Modified from Jiang et al. (2008)	(Zhai et al., 2013)
	Oct. 10–24, 2003	A,B,C	Shiyan 3	Modified from Zhai et al. (2005)	(Zhai et al., 2013)
	Oct. 1–2, 2004	A	Shiyan 3	Modified from Zhai et al. (2005)	(Zhai et al., 2013)
	Oct. 1–6, 2006	A,B	Kexue 3	Modified from Jiang et al. (2008)	(Zhai et al., 2013)
	Oct. 25–31, 2010	A	Dongfanghong 2	GO-8050	This study
	Nov. 11–16, 2002	A	Yanping 2	Zhai et al. (2005)	(Zhai et al., 2005)
	Nov. 25–30, 2006	A,B	Dongfanghong 2	Modified from Jiang et al. (2008)	(Zhai et al., 2013)
	Nov. 1–26, 2010	A,B	Dongfanghong 2	GO-8050	This study

*,# : The data collected from July 27-August 7 were published in Lv et al. (2018).

noaa.gov/gmd/dv/site/) was adopted in the atmospheric pCO_2 calculation after comparison with field measured values during the surveys.

Water pCO_2^{Eq} obtained from Formula (1) was corrected to pCO_2 at *in situ* temperatures (*in situ* pCO_2, or pCO_2 hereafter) using the empirical formula of Takahashi et al. (1993), where t is the temperature in the equilibrator in °C. Units of SST are also °C.

$$In\ situ\ pCO_2 = pCO_2^{Eq} \times \exp(0.0423 \times (SST - t)) \quad (2)$$

The net CO_2 flux (F_{CO2}) between surface water and the atmosphere (or air-sea CO_2 flux) was calculated using the following formula:

$$F_{CO2} = k \times s \times \Delta pCO_2 \quad (3)$$

where s is the solubility of CO_2 (Weiss, 1974), ΔpCO_2 is the pCO_2 difference between the surface water and the atmosphere, and k is the CO_2 transfer velocity. k was parameterized using the empirical function of Sweeney et al. (2007), and nonlinear corrections of gas transfer velocity with wind speed was adopted following Wanninkhof et al. (2002) and Jiang et al. (2008):

$$k = 0.27 \times C_2 \times U_{mean}^2 \times (Sc/660)^{-0.5} \quad (4)$$

$$C_2 = \left(\frac{1}{n}\sum_{j=1}^{n} U_j^2\right)/U_{mean}^2 \quad (5)$$

where U_{mean} is the monthly mean wind speed at 10 m above sea level (in m s^{-1}), and Sc is the Schmidt number at *in situ* temperatures for surface seawater (Wanninkhof, 1992). C_2 is the nonlinear coefficient for the quadratic term of the gas transfer relationship, U_j is the high-frequency wind speed (in m s^{-1}), the subscript "mean" indicates average values, and n is the number of available wind speed measurements for the month.

Daily sea surface wind datasets from 2000 to 2018 were acquired from the Jet Propulsion Laboratory Cross-Calibrated Multiple Platforms (CCMP) products with a spatial resolution of 0.25° (ftp://podaac-ftp.jpl.nasa.gov/allData/ccmp/L3.5a/). The monthly average wind speeds and corresponding C_2 values were generated for the five domains. As defined here, a positive flux indicates evasion of CO_2 from the sea to the atmosphere.

pCO_2 normalized to a constant temperature of 26 °C (the annually averaged SST around Dongsha Island), $NpCO_2$, was calculated following Takahashi et al. (1993):

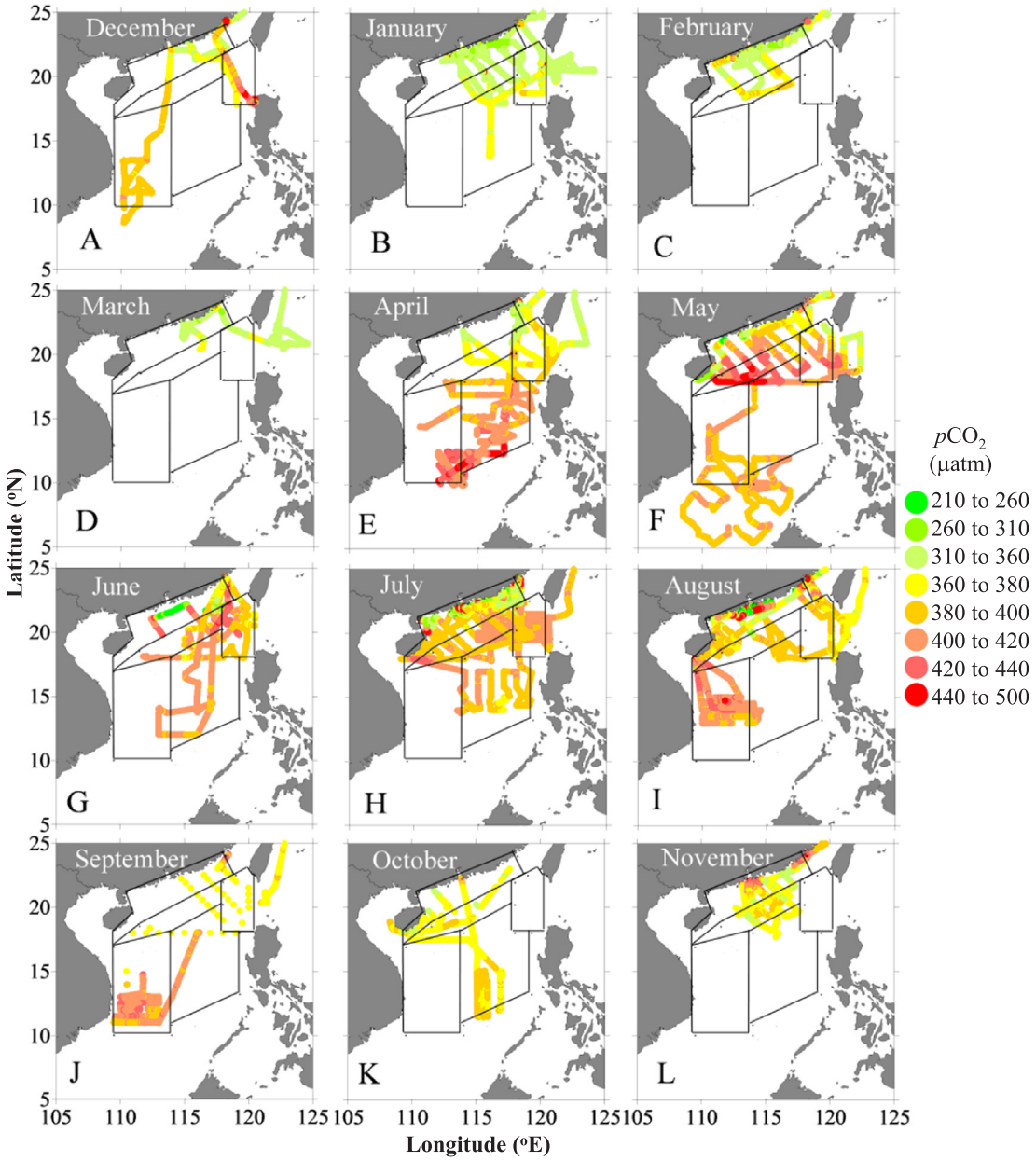

Fig. 2. Monthly spatial distributions of surface water pCO_2 in the South China Sea during the 12-month surveys of 2000 to 2018. The data were normalized to 2010 (see detail in the text).

$$NpCO_2 = pCO_2 \times \exp(0.0423 \times (26 - SST)) \quad (6)$$

Our surveys covered all four seasons of the year, among which we defined March to May as spring, June to August as summer, September to November as fall and December to February as winter.

Both atmospheric and surface seawater pCO_2 are increasing at the global scale, and the rates differ across regions (Takahashi et al., 2009). The rate of increase of xCO_2 in the atmosphere at Hawaii and Guam was 2.1 ppm yr^{-1} based on data collected from 2000 to 2017 (http://www.esrl.noaa.gov/gmd/dv/site/; http://scrippsco2.ucsd.edu/data). The rate of increase of atmospheric xCO_2 over Dongsha Island in the NSCS is 2.2 ppm yr^{-1} based on data collected from 2010 to 2017, which is the same as observed in the air over the NSCS basin, based on data collected from cruises during 1999–2008 (Sheu et al., 2010) and also the long-term observations at Hawaii and Guam. For the rate of increase of seawater pCO_2 in the SCS, there are no reports based on long-term observations. Sheu et al. (2010) observed rates of 2.5 μatm yr^{-1} based on data collected from cruises in 1989–2002, and 3.2 μatm yr^{-1} based on 1999–2008 data. The rate of seawater pCO_2 increase in the North Pacific (at HOT, the Hawaii Ocean Time-series station) is 3.2 μatm yr^{-1} based on data collected in 1997–2001 (Takahashi et al., 2009). However, this estimated rate is reduced to 1.9 μatm yr^{-1} when based on data collected over a longer time-period (1989–2015), which is almost the same as the observed rate of increase in atmospheric pCO_2 (1.9 μatm yr^{-1}, http://hahana.soest.hawaii.edu/). Similarly, the rates of increase of seawater and atmospheric pCO_2 in the North Atlantic are also very close (1.9 μatm yr^{-1} in seawater and 1.8 μatm yr^{-1} in air, http://bats.bios.edu/). This suggests that the increase in seawater pCO_2 is mainly dominated by the increase in atmospheric pCO_2. As there are no long-term observations of seawater pCO_2 in the SCS, we adopted the rate of increase of air xCO_2 to correct the seawater pCO_2. We thus corrected the surface water pCO_2 values to a reference year of 2010 using the rates of increase of 2.0 μatm yr^{-1} that we obtain when comparing pCO_2 values collected in different years. However, for air-sea CO_2 flux estimations, no time-normalization was adopted.

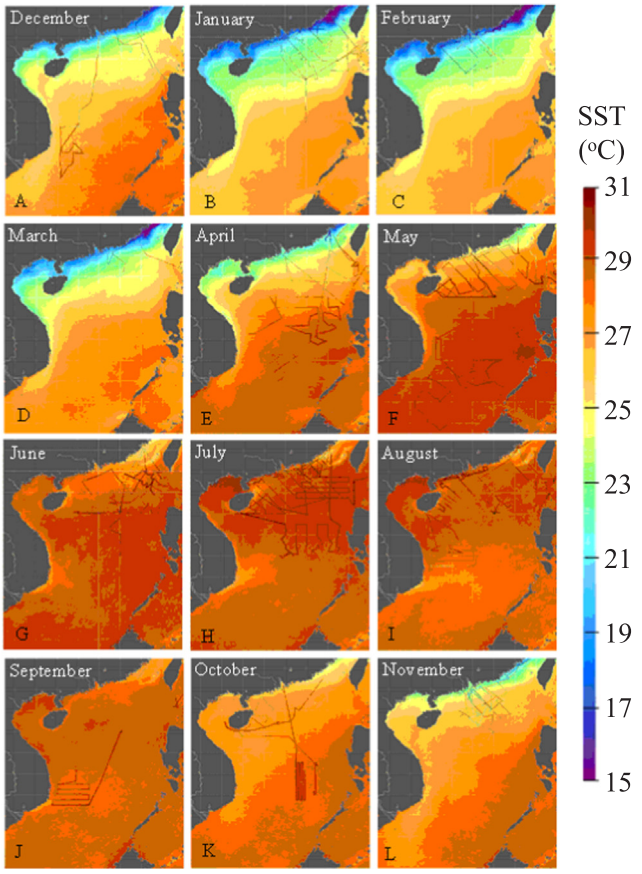

Fig. 3. Monthly spatial distributions of sea surface temperature (SST) in the South China Sea during the 12-month surveys of 2000 to 2018. Satellite-derived (from 2003 to 2016) monthly mean SSTs were calculated based on monthly mean SST values obtained from the NASA ocean color website (http://oceancolor.gsfc.nasa.gov), which were retrieved with the Moderate Resolution Imaging Spectroradiometer (MODIS) onboard the Aqua satellite. The 4 μm nighttime SST products were used here. The SST data shown in the cruise tracks were measured during the surveys.

4. Results and discussion

4.1. SST and SSS

Fig. 3 reveals the average temporal and spatial variations in SST over the 12 months of the year from 2000 to 2018. Generally, the SST distributions measured during the cruises were consistent with satellite-derived monthly mean SSTs. The seasonal variations in average SST and SSS in the five domains are further shown in Fig. 4 and Tables 3–7. In the NSCS, SST showed significant seasonal variability with high values in summer and low values in winter. In winter and early spring, SST increased offshore and from north to south with a range of ~15 to 30 °C. In the middle and southern SCS, the seasonal variability was much smaller with a range of ~27–30 °C, although SSTs were also higher in summer than in winter. The average SST values during each survey were generally consistent with expected seasonal and spatial patterns, except that the SST in Domain A during the February 2018 cruise was much lower than remotely-sensed multi-year average, attributed to the fact that only the colder coastal area was surveyed during this cruise (Figs. 2C and 4A). In summer and fall, SSTs were high and relatively spatially homogeneous compared to winter and spring, with a range of ~28–30 °C. On a monthly time-scale, the lowest SSTs appeared in January to March and the highest in June to September (Fig. 3). The magnitude of seasonal variations in SST decreased moving southward, from 6 to 10 °C in Domains A and B to ~3 °C in Domain E. The average SST measured during the surveys over the entire study area was 24.7 ± 0.5 °C in winter, 27.9 ± 0.3 °C in spring, 29.3 ± 0.3 °C in summer and 28.6 ± 0.3 °C in fall.

Generally, Domain A showed large seasonal variability with respect to salinity, with relatively low SSS in summer and early fall (< 33.0) and high SSS in winter (33.5–34.0). In Domain B, although there was a similar seasonal pattern, the SSS range was smaller (33.4–34.4). SSS in Domains C and E did not show the seasonal pattern, with a range of 33.3–33.9. SSS values in Domain A in May 2001, July 2008 and August 2015 were lower than the multi-cruise average SSS (Fig. 4B), which might be the result of influences of river discharge, wind fields, or an uneven distribution of the cruise tracks. The average SSS measured during the surveys across the entire study area was 33.7 ± 0.2 in winter, 33.8 ± 0.3 in spring, 33.3 ± 0.4 in summer and 33.3 ± 0.3 in fall.

4.2. Wind speeds and C_2

The temporal patterns of wind speed in the five domains were similar (Fig. 4C). Monthly average wind speeds ranged from 4.0 to 12.3 m s^{-1}, and their standard deviations (SDs) were lower than 0.1 m s^{-1}. Generally, wind speeds were high in fall and winter but low in spring and summer, with inter-annual variations observed. The highest wind speeds were recorded in Domains B and D in December 2006 and Domain D in December 2008, when the monthly average wind speeds reached > 12 m s^{-1}. The lowest wind speeds were observed in Domain C in May 2011 and May 2014, when the monthly average wind speeds were < 5 m s^{-1}.

The resulting C_2 values ranged from 1.03 to 1.52, with higher values in spring, summer and fall and relatively lower values in winter (Tables 3–7). The average C_2 values during the four seasons were 1.10 ± 0.02, 1.20 ± 0.03, 1.21 ± 0.08 and 1.20 ± 0.03 in winter, spring, summer and fall, respectively. The C_2 values in the SCS were similar to those in the East China Sea (~1.20, Guo et al. (2015)) and slightly lower than the global average of 1.27 (Wanninkhof et al., 2009).

4.3. CO_2 mole fraction in the air

Field-observed xCO_2 in the air over the NSCS (on the Dong-Sha Island, 116.73 °E, 20.0 °N) showed an increasing trend with seasonal variations of ~20 ppm. Although the observed trend was similar to that found over the North Pacific (Hawaii and Guam), the magnitude of seasonal variability in the xCO_2 over the NSCS was larger (Fig. 5), which might suggest stronger anthropogenic impacts in marginal seas than in the open ocean. Both the seasonal and inter-annual patterns we observed during the surveys were similar to those found in the North Pacific and Dong-Sha Island in the NSCS, with the highest values typically observed in spring and the lowest values in fall (Fig. 5). The differences in atmospheric xCO_2 between our shipboard measurements over the SCS and those observed over Hawaii were not significant, ranging from 0.7 to 10.3 ppm (average ~4.0 ppm).

4.4. Surface seawater pCO_2 and its major controls

pCO_2 values along the cruise tracks are shown in Fig. 2. By averaging the pCO_2 values along these tracks over 1° × 1° grids, we obtained the mean pCO_2 values of the five domains (Tables 3–7 and Fig. 6).

In Domain A, surface water pCO_2 in summer showed highly variable range of 150–650 μatm under the impact of both phytoplankton blooms in the Pearl River plume and CO_2-replete subsurface water in the nearshore upwelling system. The pCO_2 values in this domain in winter were generally low. In Domain B in the NSCS slope, surface water pCO_2 was low in winter and early spring (300–360 μatm) but high in late spring and summer (> 380 μatm). In the SCS basin (Domain C), pCO_2 was high (380–500 μatm) in throughout spring, summer and fall but relatively low in winter, based on limited data in winter. In Domain D,

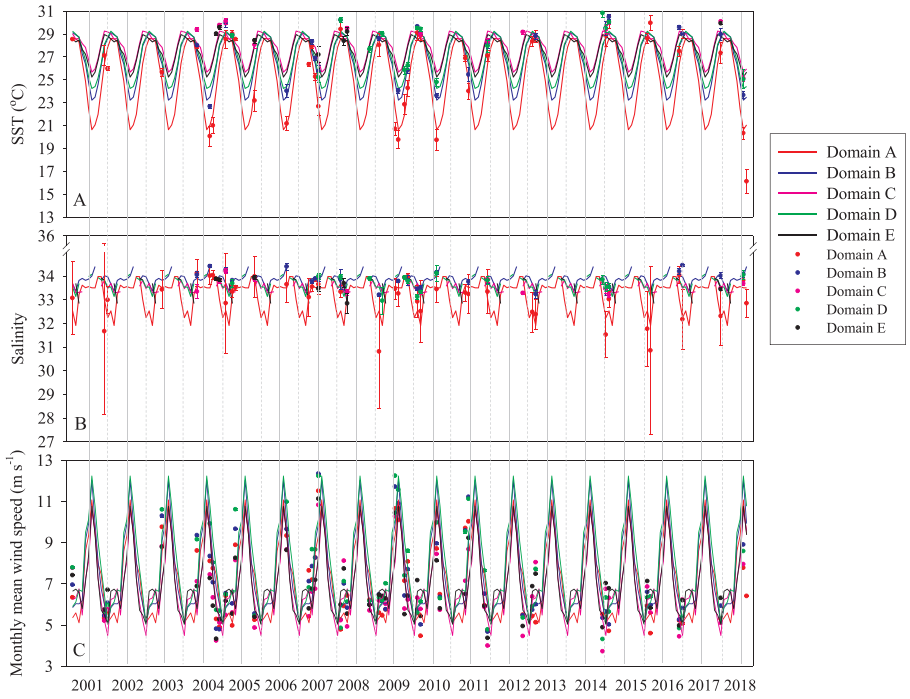

Fig. 4. Sea surface temperature (SST, A), sea surface salinity (SSS, B) and wind speed (C) in the five domains in the South China Sea. The solid lines are the multi-year average values and the dots are the averages during the surveys (for SST and SSS) or monthly averages (for wind speed). The multi-year averages of SST (see details in caption of Fig. 3) and wind speeds (see detail in the text) were calculated from the remote sensing data and SSS were from the surveys (data presented in Tables 3–7). The error bars show the standard deviations. The vertical solid lines show January and the dashed lines show July of each year.

both surface water pCO_2 values and seasonal patterns were similar with that of Domain B except in the area off northwest Luzon during the winter upwelling season when pCO_2 reached 470 µatm. In the WSCS off Vietnam (Domain E), pCO_2 was higher in surface water than in the atmosphere during all surveyed seasons (380–440 µatm), with the exception in October 2003 when surface water pCO_2 (349–406 µatm) was similar to atmospheric pCO_2 and was overall much lower than during other seasons (Fig. 2K).

The seasonal average ΔpCO_2 ranged from −176 to 160 µatm. Low values were observed in Domains A and B in winter, and in Domain A in spring and summer in the Pearl River plume. High values were seen in Domains C and E in spring, summer and fall, and upwelling areas in Domain A in summer (Fig. 6).

Zhai et al. (2005; 2013) suggested that surface water pCO_2 in the SCS was dominated by SST based on the data collected in 2000–2008. With the data collected in 2009–2018 integrated, we use similar methods to reveal pCO_2 controlling mechanisms.

Figs. 7–9 show the relationship between pCO_2 and SST and between $NpCO_2$ and SSS in the 5 domains. In Domain A, pCO_2 ranged from 150 to 650 µatm. In winter, early spring and late fall (the low SST seasons), pCO_2 was generally higher than the SST-dominated pCO_2 range (shown as two dashed lines in the figures) and $NpCO_2$ was the highest among the surveyed months. In addition, lower SSTs generally had higher pCO_2 deviations from the SST-dominated pCO_2 range, suggesting stronger vertical mixing in cold seasons or areas. These low SSTs resulted in low *in situ* pCO_2 and negative ΔpCO_2 in winter as shown in Fig. 7A-1, A-2, A-3 and Fig. 6. In late spring (May), the area impacted by the Pearl River plume had pCO_2 values lower than the SST-dominated pCO_2 range, and $NpCO_2$ was very low (Fig. 7B-1 and B-2). In summer, the pCO_2 of the nearshore area was high (up to 650 µatm), influenced by coastal upwelling as previously observed (Cao et al., 2011), while the area influenced by the Pearl River plume had values as low as 150 µatm. As a result, a lowest $NpCO_2$ among all domains was observed in Domain A (Fig. 7C-1 and C-2). In fall, most pCO_2 values were above the SST-dominated pCO_2 range and $NpCO_2$ was higher than in late spring and summer (Fig. 7D-1 and D-2). This revealed that during cold seasons (late fall to early spring) the vertical mixing of subsurface CO_2-replete water was a major control on surface water pCO_2. However, during warm seasons (late spring and summer), the influence of low-pCO_2 plume water was the most important factor. Additionally, temperature effect was important in regulating the *in situ* pCO_2 in all seasons. Taken together, pCO_2 in Domain A was primarily modulated by vertical mixing and cooling in cold seasons, and by biological drawdown stimulated by the Pearl River plume and warming in warm seasons. Summer coastal upwelling may also induce high pCO_2 though it was limited to a very nearshore area.

In Domain B, the pCO_2 range was much smaller (280–400 µatm). In winter, the pCO_2 values were slightly higher than or within the SST-dominated pCO_2 range. $NpCO_2$ in winter was the highest among the seasons (Fig. 8A-1 and A-2). In spring, pCO_2 values were within the SST-dominated pCO_2 range (Fig. 8B-1), and $NpCO_2$ was slightly lower than in winter. Additionally, $NpCO_2$ increased overall along with higher SSS, suggesting pCO_2 drawdown in the plume (the lower salinity zone, Fig. 8B-2). In summer, most pCO_2 values were within or lower than the SST-dominated pCO_2 range (Fig. 8C-1). Generally, $NpCO_2$ increased with salinity, suggesting strong pCO_2 reduction in the Pearl River plume (Fig. 8C-2). In fall, pCO_2 values were within or just outside the SST-dominated pCO_2 range (Fig. 8D-1), and areas with the highest pCO_2 also had the highest $NpCO_2$ values suggesting the contribution of vertical mixing. In summary, pCO_2 in Domain B was mainly dominated by SST, although the influence of CO_2-replete subsurface water in winter and late fall and CO_2-depleted Pearl River plume in summer also played important roles.

In Domain C, most pCO_2 values were within or just outside the SST-dominated pCO_2 range (Fig. 9A-1). Generally, $NpCO_2$ showed no pattern with salinity (Fig. 9A-2), suggesting that pCO_2 in this domain was mainly dominated by variations in SST and had little influence by the Pearl River plume. In Domain D, pCO_2 in the northwestern corner in summer was still influenced by the Pearl River plume and pCO_2 values were lower than the SST-dominated pCO_2 range. However, pCO_2 in winter (December 2006 and January 2018) was strongly influenced by upwelling, and values were higher than the SST-dominated pCO_2 range (Fig. 9B-1). The northwestern corner, with low pCO_2 in summer, had the lowest $NpCO_2$ values, and the winter upwelling region had the highest $NpCO_2$ values among Domains C, D and E (Fig. 9). In Domain E, pCO_2 values were generally within or just outside the SST-dominated pCO_2 range (Fig. 9C-1). The southwestern corner of Domain E in September 2007 was influenced by the Mekong River plume and SSS was

Table 3
pCO_2, CO_2 fluxes and other parameters in Domain A during the surveys (Temp. is temperature; Atm. pCO_2 is atmospheric pCO_2).

Season	Survey period	Temp. (°C)		Salinity		Water pCO_2 (μatm)		Atm. pCO_2 (μatm)		ΔpCO_2 (μatm)		FCO_2 (mmol m^{-2} d^{-1})		Wind speed (m s^{-1})		C_2
		Mean	SD	Mean	SD	Mean	SD	Mean	SD	Mean	SD	Mean	SD	Mean	SD	
Winter	Dec. 1–23, 2006	22.68	0.76	33.65	0.44	370.8	14.5	378.8	1.5	−8.1	14.6	−2.5	4.9	11.50	0.02	1.04
	Dec. 29–31, 2008	20.70	0.57	33.46	0.46	340.0	15.1	378.3	1.4	−38.3	15.1	−10.4	5.1	10.65	0.03	1.06
	Jan. 1–11, 2009	19.77	0.78	33.26	0.55	331.8	16.0	379.2	1.3	−47.4	16.1	−11.8	4.8	10.09	0.03	1.07
	Jan. 5–31, 2010	19.74	0.92	33.44	0.54	320.9	11.1	381.3	1.4	−59.6	11.2	−11.4	4.1	8.71	0.03	1.10
	Jan. 4–31, 2018	20.33	0.52	33.81	0.20	348.9	5.2	400.2	1.4	−51.3	5.4	−7.9	2.7	7.77	0.01	1.12
	Feb. 10–29, 2004	20.07	0.89	34.01	0.35	333.4	8.6	370.8	1.5	−37.5	8.7	−6.5	2.0	8.10	0.03	1.17
	Feb. 15–20, 2006	21.17	0.60	33.64	0.78	370.5	26.0	375.6	1.3	−5.9	26.1	−1.3	3.5	9.33	0.03	1.12
	Feb. 1–4, 2018	16.12	1.02	32.85	0.60	339.2	12.2	404.7	0.9	−65.5	12.2	−7.5	2.3	6.40	0.02	1.20
	Seasonal average	**20.07**	**0.78**	**33.52**	**0.52**	**344.4**	**14.8**	**383.6**	**1.4**	**−39.2**	**14.8**	**−7.4**	**3.9**	**9.07**	**0.03**	**1.11**
Spring	Mar. 1–5, 2004	21.01	0.70	34.03	0.19	333.9	8.0	370.6	1.4	−36.7	8.1	−5.9	2.2	7.74	0.03	1.18
	Mar. 20–31, 2009	22.84	0.89	33.94	0.07	333.4	5.1	377.6	1.1	−44.1	5.2	−6.1	2.1	7.15	0.03	1.20
	Apr. 29, 2004	–	–	–	–	–	–	–	–	–	–	–	–	–	–	–
	Apr. 10–25, 2005	23.18	0.94	33.98	0.86	343.9	13.6	373.2	1.3	−29.3	13.7	−2.2	1.5	5.25	0.02	1.20
	Apr. 20–30, 2008	–	–	–	–	–	–	–	–	–	–	–	–	–	–	–
	Apr. 1–21, 2009	24.27	0.70	33.98	0.14	353.5	6.6	375.8	1.2	–22.4	6.7	−3.9	2.9	8.08	0.04	1.18
	Apr. 30, 2011	–	–	–	–	–	–	–	–	–	–	–	–	–	–	–
	Apr. 9–29, 2012	–	–	–	–	–	–	–	–	–	–	–	–	–	–	–
	May 14–30, 2001	27.11	0.85	31.66	3.52	332.0	52.3	360.8	0.4	−28.8	52.3	−2.3	3.8	5.33	0.03	1.23
	May 1–28, 2004	–	–	–	–	–	–	–	–	–	–	–	–	–	–	–
	May 1–29, 2011	27.10	0.49	33.33	0.93	382.7	22.3	378.6	1.0	4.1	22.3	0.2	1.5	4.73	0.02	1.22
	May 23–31, 2014	–	–	–	–	–	–	–	–	–	–	–	–	–	–	–
	May 15–31, 2016	27.50	0.41	34.03	0.35	397.7	14.1	393.0	1.4	4.6	14.2	0.3	2.4	5.22	0.02	1.18
	Seasonal average	**24.72**	**0.74**	**33.56**	**1.43**	**353.9**	**23.14**	**375.7**	**1.16**	**−21.8**	**23.2**	**−2.8**	**2.5**	**6.21**	**0.03**	**1.20**
Summer	Jun. 2–3, 2001	25.98	0.16	32.99	0.58	381.0	13.3	359.4	0.5	21.6	13.3	1.7	0.9	5.59	0.02	1.14
	Jun. 1–20, 2014	28.83	0.90	31.52	0.97	305.8	47.9	381.2	1.4	−75.5	47.9	−6.1	6.4	5.39	0.02	1.20
	Jun. 1–5, 2016	29.01	0.37	32.17	1.26	374.8	37.6	391.2	0.5	−16.4	37.6	−1.2	5.6	5.07	0.04	1.18
	Jun. 5–27, 2017	27.33	0.90	32.30	1.23	366.9	16.7	392.2	1.3	−25.3	16.8	−1.8	1.9	5.29	0.01	1.14
	Jul. 10–21, 2000	28.54	0.12	33.07	1.54	420.6	30.9	356.1	0.1	64.5	30.9	6.9	2.3	6.34	0.03	1.19
	Jul 6–23, 2004	28.55	0.80	32.85	2.10	359.8	32.4	361.8	0.9	−2.0	32.4	−0.2	2.0	6.41	0.02	1.13
	Jul. 1–24, 2007	29.42	0.64	33.33	0.25	373.6	12.0	366.1	1.2	7.5	12.0	0.5	1.9	4.78	0.02	1.22
	Jul. 1–14, 2008	28.03	0.99	30.81	2.41	355.9	41.1	369.8	0.6	−13.8	41.1	−1.2	2.9	5.59	0.02	1.18
	Jul. 17–31, 2009	29.11	0.68	32.92	0.68	366.7	38.9	368.7	0.6	−2.0	38.9	−0.2	3.0	5.57	0.02	1.17
	Jul. 29–31, 2012	28.35	0.42	32.48	0.85	371.4	20.9	373.3	0.3	−1.9	20.9	−0.2	1.1	5.43	0.02	1.18
	Jul. 1–18, 2014	30.07	0.58	33.02	0.33	394.6	15.2	378.1	0.2	16.5	15.2	1.0	1.9	4.71	0.02	1.25
	Jul. 19–31, 2015	28.62	0.48	31.77	1.58	385.8	60.3	382.0	0.6	3.8	60.4	0.4	5.8	5.91	0.03	1.20
	Aug. 14–31, 2007	–	–	–	–	–	–	–	–	–	–	–	–	–	–	–
	Aug. 6–31, 2008	–	–	–	–	–	–	–	–	–	–	–	–	–	–	–
	Aug. 1–18, 2009	28.84	0.43	32.51	1.31	379.1	32.4	367.8	4.5	−42.8	32.7	−3.9	11.6	4.47	0.03	1.44
	Aug. 1–21, 2012	28.78	0.54	32.38	0.64	378.6	30.1	372.9	0.7	5.6	30.1	0.4	2.0	5.13	0.03	1.29
	Aug. 1–8, 2015	29.97	0.68	30.85	3.55	388.3	103.1	378.1	0.6	10.2	103.1	0.6	2.7	4.59	0.02	1.26
	Seasonal average	**28.63**	**0.63**	**32.33**	**1.54**	**373.5**	**42.0**	**373.3**	**1.4**	**−3.3**	**42.0**	**−0.2**	**4.4**	**5.35**	**0.03**	**1.21**
Fall	Sep. 18–30, 2004	29.02	0.28	33.34	0.25	360.6	2.8	355.1	0.4	5.4	2.8	0.4	0.3	4.97	0.03	1.24
	Sep. 30, 2006	26.35	0.18	33.11	0.80	404.8	36.6	365.6	0.0	39.2	36.6	6.1	4.9	7.64	0.03	1.19
	Sep. 1–14, 2007	–	–	–	–	–	–	–	–	–	–	–	–	–	–	–
	Oct. 10–24, 2003	27.89	0.11	34.12	0.57	361.6	7.0	358.1	0.2	3.5	7.0	0.7	2.0	8.61	0.03	1.12
	Oct. 1–2, 2004	28.55	0.07	33.50	0.09	359.7	1.7	355.8	0.1	3.9	1.7	0.8	1.5	8.88	0.03	1.11
	Oct. 1–6, 2006	27.96	0.17	33.55	0.19	365.1	4.2	364.3	0.6	0.9	4.2	0.1	1.3	7.19	0.03	1.19
	Oct. 25–31, 2010	26.88	0.24	33.30	0.35	365.2	5.1	376.2	0.6	−11.0	5.1	−2.6	1.6	9.70	0.04	1.12
	Nov. 11–16, 2002	25.66	0.36	33.43	0.81	395.0	19.1	360.2	0.5	34.8	19.1	8.2	3.1	9.76	0.03	1.10
	Nov. 25–30, 2006	25.26	0.33	33.86	0.10	363.6	6.5	375.7	0.6	−12.1	6.5	−2.1	2.3	8.26	0.03	1.15
	Nov. 1–26, 2010	24.01	0.68	33.23	0.82	374.3	17.9	377.5	1.1	−3.2	17.9	−0.8	4.8	10.03	0.02	1.05
	Seasonal average	**26.84**	**0.32**	**33.49**	**0.53**	**372.2**	**15.5**	**365.4**	**0.5**	**6.8**	**15.5**	**1.2**	**2.8**	**8.34**	**0.03**	**1.14**

Table 4
pCO_2, CO_2 fluxes and other parameters in Domain B during the surveys (Temp. is temperature; Atm. pCO_2 is atmospheric pCO_2).

Season	Survey period	Temp. (°C)		Salinity		Water pCO_2 (μatm)		Atm. pCO_2 (μatm)		ΔpCO_2 (μatm)		FCO_2 (mmol m^{-2} d^{-1})		Wind speed (m s^{-1})		C_2
		Mean	SD	Mean	SD	Mean	SD	Mean	SD	Mean	SD	Mean	SD	Mean	SD	
Winter	Dec. 1–23, 2006	25.75	0.50	33.87	0.11	375.5	7.2	376.9	0.4	−1.4	7.2	−0.5	3.5	12.34	0.03	1.03
	Dec. 29–31, 2008	–	–	–	–	–	–	–	–	–	–	–	–	–	–	–
	Jan. 1–11, 2009	24.04	0.22	33.79	0.06	350.0	4.6	376.7	0.2	−26.7	4.6	−7.6	1.5	10.89	0.04	1.07
	Jan. 5–31, 2010	23.62	0.16	34.15	0.08	350.7	29.1	379.2	0.4	−28.5	29.1	−5.7	2.8	8.95	0.04	1.11
	Jan. 4–31, 2018	23.66	0.32	34.08	0.14	377.3	3.5	396.2	0.2	−18.9	3.5	−3.7	0.1	8.90	0.02	1.09
	Feb. 10–29, 2004	22.66	0.18	34.41	0.06	342.6	4.1	369.5	0.3	−26.9	4.1	−4.7	0.7	8.34	0.04	1.13
	Feb. 15–20, 2006	24.03	0.55	34.40	0.15	372.3	8.2	373.9	0.4	−1.6	8.2	−0.5	1.8	9.65	0.05	1.11
	Feb. 1–4, 2018	–	–	–	–	–	–	–	–	–	–	–	–	–	–	–
	Seasonal average	**23.96**	**0.35**	**34.12**	**0.11**	**361.4**	**13.0**	**378.7**	**0.3**	**−17.3**	**13.0**	**−3.8**	**2.1**	**9.85**	**0.04**	**1.09**
Spring	Mar. 1–5, 2004	24.36	0.09	34.02	0.02	354.8	1.4	368.6	1.4	−13.9	1.4	−1.9	0.2	7.07	1.24	1.24
	Mar. 20–31, 2009	–	–	–	–	–	–	–	–	–	–	–	–	–	–	–
	Apr. 29, 2004	28.83	0.23	33.94	0.11	388.5	3.2	363.3	0.2	25.2	3.2	1.6	0.2	4.81	0.03	1.21
	Apr. 10–25, 2005	–	–	–	–	–	–	–	–	–	–	–	–	–	–	–
	Apr. 20–30, 2008	–	–	–	–	–	–	–	–	–	–	–	–	–	–	–
	Apr. 1–21, 2009	25.83	0.31	33.81	0.20	368.3	2.8	374.8	0.4	−6.5	2.8	−1.0	1.1	7.71	0.05	1.18
	Apr. 30, 2011	–	–	–	–	–	–	–	–	–	–	–	–	–	–	–
	Apr. 9–29, 2012	27.61	0.30	33.97	0.17	402.0	3.7	380.5	0.3	21.5	3.7	1.7	0.3	5.47	0.03	1.19
	May 14–30, 2001	28.44	0.10	33.68	0.10	414.9	7.6	360.0	0.0	55.0	7.6	4.5	0.1	5.45	1.68	1.22
	May 1–28, 2004	–	–	–	–	–	–	–	–	–	–	–	–	–	–	–
	May 1–29, 2011	28.14	0.41	33.84	0.14	407.2	6.4	377.8	0.8	29.5	6.5	1.7	0.8	4.67	0.03	1.17
	May 23–31, 2014	–	–	–	–	–	–	–	–	–	–	–	–	–	–	–
	May 15–31, 2016	29.58	0.19	34.20	0.14	450.3	6.1	391.2	0.3	59.0	6.1	4.2	0.8	5.26	0.03	1.13
	Seasonal average	**27.54**	**0.26**	**33.92**	**0.14**	**398.0**	**4.9**	**373.7**	**0.7**	**24.3**	**4.9**	**1.5**	**0.6**	**5.78**	**0.79**	**1.19**
Summer	Jun. 2–3, 2001	–	–	–	–	–	–	–	–	–	–	–	–	–	–	–
	Jun. 1–20, 2014	29.48	0.59	33.45	0.29	404.6	19.3	380.7	0.8	23.9	19.3	1.9	1.7	5.65	0.02	1.10
	Jun. 1–5, 2016	29.02	0.14	34.45	0.03	428.9	6.8	391.2	0.3	37.7	6.8	3.3	1.0	5.82	0.06	1.16
	Jun. 5–27, 2017	28.97	0.49	34.01	0.12	413.6	6.4	391.1	0.6	22.5	6.4	2.0	0.6	5.93	0.02	1.15
	Jul. 10–21, 2000	–	–	–	–	–	–	–	–	–	–	–	–	–	–	–
	Jul 6–23, 2004	29.93	0.32	34.26	0.11	381.7	4.6	360.6	0.4	21.1	4.6	2.3	0.7	6.54	0.03	1.14
	Jul. 1–24, 2007	30.22	0.23	33.85	0.42	395.2	16.3	365.4	0.1	29.7	16.3	2.3	1.3	5.25	0.04	1.24
	Jul. 1–14, 2008	28.62	0.19	33.20	0.07	404.7	4.0	369.3	0.2	35.4	4.0	3.8	0.2	6.48	0.03	1.14
	Jul. 17–31, 2009	29.66	0.10	33.45	0.07	393.1	1.7	368.3	0.1	24.8	1.7	2.2	0.2	5.74	0.03	1.16
	Jul. 29–31, 2012	–	–	–	–	–	–	–	–	–	–	–	–	–	–	–
	Jul. 1–18, 2014	30.48	0.21	33.55	0.07	422.8	4.3	377.7	0.1	45.1	4.3	3.1	0.2	5.02	0.03	1.21
	Jul. 19–31, 2015	–	–	–	–	–	–	–	–	–	–	–	–	–	–	–
	Aug. 14–31, 2007	–	–	–	–	–	–	–	–	–	–	–	–	–	–	–
	Aug. 6–31, 2008	–	–	–	–	–	–	–	–	–	–	–	–	–	–	–
	Aug. 1–18, 2009	29.11	0.14	33.51	0.08	390.9	2.0	365.8	0.2	25.1	2.0	2.2	0.2	5.02	0.05	1.52
	Aug. 1–21, 2012	28.81	0.26	33.23	0.16	393.9	6.7	372.9	0.4	21.0	6.7	2.1	0.8	6.00	0.04	1.22
	Aug. 1–8, 2015	–	–	–	–	–	–	–	–	–	–	–	–	–	–	–
	Seasonal average	**29.43**	**0.31**	**33.70**	**0.18**	**402.9**	**9.1**	**374.3**	**0.40**	**28.6**	**9.1**	**2.5**	**0.9**	**5.74**	**0.04**	**1.20**
Fall	Sep. 18–30, 2004	28.91	0.11	33.82	0.04	364.4	1.6	355.3	0.2	9.2	1.6	0.9	0.3	6.04	0.03	1.16
	Sep. 30, 2006	–	–	–	–	–	–	–	–	–	–	–	–	–	–	–
	Sep. 1–14, 2007	–	–	–	–	–	–	–	–	–	–	–	–	–	–	–
	Oct. 10–24, 2003	28.02	0.07	34.05	0.13	355.1	0.9	358.0	0.3	−2.8	1.0	−0.6	0.4	9.35	0.04	1.09
	Oct. 1–2, 2004	–	–	–	–	–	–	–	–	–	–	–	–	–	–	–
	Oct. 1–6, 2006	28.34	0.20	33.76	0.06	367.0	3.9	364.0	0.1	3.1	3.9	0.5	1.1	7.86	0.04	1.12
	Oct. 25–31, 2010	–	–	–	–	–	–	–	–	–	–	–	–	–	–	–
	Nov. 11–16, 2002	–	–	–	–	–	–	–	–	–	–	–	–	–	–	–
	Nov. 25–30, 2006	26.89	0.19	33.89	0.05	370.8	3.5	374.8	0.8	−3.9	3.5	−0.7	0.4	8.27	0.05	1.19
	Nov. 1–26, 2010	25.46	0.62	33.76	0.11	369.7	5.2	376.6	0.5	−6.9	5.3	−2.0	1.8	11.22	0.03	1.03
	Seasonal average	**27.52**	**0.31**	**33.85**	**0.09**	**365.4**	**3.4**	**365.7**	**0.5**	**−0.3**	**3.4**	**−0.4**	**1.0**	**8.55**	**0.04**	**1.12**

Table 5
pCO_2, CO_2 fluxes and other parameters in Domain C during the surveys (Temp. is temperature; Atm. pCO_2 is atmospheric pCO_2).

Season	Survey period	Temp. (°C)		Salinity		Water pCO_2 (μatm)		Atm. pCO_2 (μatm)		ΔpCO_2 (μatm)		FCO_2 (mmol m^{-2} d^{-1})		Wind speed (m s^{-1})		C_2
		Mean	SD	Mean	SD	Mean	SD	Mean	SD	Mean	SD	Mean	SD	Mean	SD	
Winter	Dec. 1–23, 2006	–	–	–	–	–	–	–	–	–	–	–	–	–	–	–
	Dec. 29–31, 2008	–	–	–	–	–	–	–	–	–	–	–	–	–	–	–
	Jan. 1–11, 2009	–	–	–	–	–	–	–	–	–	–	–	–	–	–	–
	Jan. 5–31, 2010	–	–	–	–	–	–	–	–	–	–	–	–	–	–	–
	Jan. 4–31, 2018	25.13	0.26	33.68	0.10	382.3	3.0	393.3	0.8	−11.1	3.1	−1.8	0.7	7.95	0.01	1.14
	Feb. 10–29, 2004	–	–	–	–	–	–	–	–	–	–	–	–	–	–	–
	Feb. 15–20, 2006	–	–	–	–	–	–	–	–	–	–	–	–	–	–	–
	Feb. 1–4, 2018	–	–	–	–	–	–	–	–	–	–	–	–	–	–	–
	Seasonal average	**25.13**	**0.26**	**33.68**	**0.10**	**382.3**	**3.0**	**393.3**	**0.8**	**−11.1**	**3.1**	**−1.8**	**0.7**	**7.9**	**0.0**	**1.14**
Spring	Mar. 1–5, 2004	–	–	–	–	–	–	–	–	–	–	–	–	–	–	–
	Mar. 20–31, 2009	–	–	–	–	–	–	–	–	–	–	–	–	–	–	–
	Apr. 29, 2004	–	–	–	–	–	–	–	–	–	–	–	–	–	–	–
	Apr. 10–25, 2005	28.06	0.33	33.86	0.08	410.4	10.6	369.7	0.6	40.7	10.6	2.7	1.0	4.86	0.02	1.23
	Apr. 20–30, 2008	–	–	–	–	–	–	–	–	–	–	–	–	–	–	–
	Apr. 1–21, 2009	–	–	–	–	–	–	–	–	–	–	–	–	–	–	–
	Apr. 30, 2011	–	–	–	–	–	–	–	–	–	–	–	–	–	–	–
	Apr. 9–29, 2012	29.17	0.19	33.28	0.08	406.9	3.3	379.1	0.7	27.8	3.3	1.5	0.3	4.46	0.01	1.17
	May 14–30, 2001	–	–	–	–	–	–	–	–	–	–	–	–	–	–	–
	May 1–28, 2004	29.77	0.15	33.77	0.08	386.5	3.2	362.6	0.3	23.9	3.3	1.8	0.3	5.12	0.02	1.25
	May 1–29, 2011	28.32	0.32	33.87	0.12	409.9	5.7	377.6	0.3	32.3	5.7	1.4	0.4	3.99	0.01	1.21
	May 23–31, 2014	–	–	–	–	–	–	–	–	–	–	–	–	–	–	–
	May 15–31, 2016	–	–	–	–	–	–	–	–	–	–	–	–	–	–	–
	Seasonal average	**28.83**	**0.26**	**33.70**	**0.09**	**403.5**	**6.5**	**372.3**	**0.5**	**31.2**	**6.3**	**1.8**	**0.6**	**4.61**	**0.02**	**1.22**
Summer	Jun. 2–3, 2001	–	–	–	–	–	–	–	–	–	–	–	–	–	–	–
	Jun. 1–20, 2014	29.38	0.35	33.46	0.19	401.4	9.7	380.8	0.2	20.6	9.7	2.4	1.0	6.74	0.02	1.12
	Jun. 1–5, 2016	–	–	–	–	–	–	–	–	–	–	–	–	–	–	–
	Jun. 5–27, 2017	30.09	0.14	33.48	0.09	418.1	2.5	389.7	0.2	28.4	2.5	2.0	0.2	5.09	0.01	1.20
	Jul. 10–21, 2000	–	–	–	–	–	–	–	–	–	–	–	–	–	–	–
	Jul 6–23, 2004	30.12	0.25	34.20	0.10	391.4	4.2	360.4	0.2	31.0	4.2	2.8	0.3	5.48	0.02	1.31
	Jul. 1–24, 2007	–	–	–	–	–	–	–	–	–	–	–	–	–	–	–
	Jul. 1–14, 2008	–	–	–	–	–	–	–	–	–	–	–	–	–	–	–
	Jul. 17–31, 2009	–	–	–	–	–	–	–	–	–	–	–	–	–	–	–
	Jul. 29–31, 2012	–	–	–	–	–	–	–	–	–	–	–	–	–	–	–
	Jul. 1–18, 2014	30.02	0.14	33.19	0.10	402.5	3.4	378.1	0.3	24.4	3.4	2.7	1.0	6.31	0.02	1.20
	Jul. 19–31, 2015	–	–	–	–	–	–	–	–	–	–	–	–	–	–	–
	Aug. 14–31, 2007	–	–	–	–	–	–	–	–	–	–	–	–	–	–	–
	Aug. 6–31, 2008	–	–	–	–	–	–	–	–	–	–	–	–	–	–	–
	Aug. 1–18, 2009	29.02	0.20	33.29	0.09	386.1	8.3	365.9	0.4	20.2	8.3	2.2	0.5	5.77	0.03	1.44
	Aug. 1–21, 2012	–	–	–	–	–	–	–	–	–	–	–	–	–	–	–
	Aug. 1–8, 2015	–	–	–	–	–	–	–	–	–	–	–	–	–	–	–
	Seasonal average	**29.73**	**0.23**	**33.53**	**0.12**	**399.9**	**6.3**	**375.0**	**0.3**	**24.9**	**6.3**	**2.4**	**0.7**	**5.88**	**0.02**	**1.25**
Fall	Sep. 18–30, 2004	–	–	–	–	–	–	–	–	–	–	–	–	–	–	–
	Sep. 30, 2006	–	–	–	–	–	–	–	–	–	–	–	–	–	–	–
	Sep. 1–14, 2007	29.50	0.12	33.31	0.14	402.0	4.3	362.9	0.1	39.1	4.3	2.8	0.3	4.93	0.02	1.32
	Oct. 10–24, 2003	29.39	0.20	33.34	0.29	365.9	4.0	356.8	0.5	9.0	4.0	1.2	1.0	7.11	0.02	1.20
	Oct. 1–2, 2004	–	–	–	–	–	–	–	–	–	–	–	–	–	–	–
	Oct. 1–6, 2006	–	–	–	–	–	–	–	–	–	–	–	–	–	–	–
	Oct. 25–31, 2010	–	–	–	–	–	–	–	–	–	–	–	–	–	–	–
	Nov. 11–16, 2002	–	–	–	–	–	–	–	–	–	–	–	–	–	–	–
	Nov. 25–30, 2006	–	–	–	–	–	–	–	–	–	–	–	–	–	–	–
	Nov. 1–26, 2010	–	–	–	–	–	–	–	–	–	–	–	–	–	–	–
	Seasonal average	**29.44**	**0.17**	**33.33**	**0.23**	**383.9**	**4.2**	**359.9**	**0.4**	**24.1**	**4.2**	**2.0**	**0.7**	**6.02**	**0.02**	**1.26**

Table 6
pCO_2, CO_2 fluxes and other parameters in Domain D during the surveys (Temp. is temperature; Atm. pCO_2 is atmospheric pCO_2).

Season	Survey period	Temp. (°C)		Salinity		Water pCO_2 (μatm)		Atm. pCO_2 (μatm)		ΔpCO_2 (μatm)		FCO_2 (mmol m^{-2} d^{-1})		Wind speed (m s^{-1})		C_2
		Mean	SD	Mean	SD	Mean	SD	Mean	SD	Mean	SD	Mean	SD	Mean	SD	
Winter	Dec. 1–23, 2006	25.21	0.42	33.98	0.12	392.7	17.0	377.3	0.5	15.4	17.0	4.4	7.2	12.23	0.04	1.06
	Dec. 29–31, 2008	–	–	–	–	–	–	–	–	–	–	–	–	–	–	–
	Jan. 1–11, 2009	–	–	–	–	–	–	–	–	–	–	–	–	–	–	–
	Jan. 5–31, 2010	24.80	0.35	34.12	0.33	383.0	98.3	378.4	0.3	4.7	98.3	1.1	15.1	9.98	0.04	1.09
	Jan. 4–31, 2018	25.04	0.83	34.04	0.18	373.4	8.2	395.0	0.7	−21.6	8.2	−4.0	2.2	8.58	0.02	1.13
	Feb. 10–29, 2004	–	–	–	–	–	–	–	–	–	–	–	–	–	–	–
	Feb. 15–20, 2006	–	–	–	–	–	–	–	–	–	–	–	–	–	–	–
	Feb. 1–4, 2018	–	–	–	–	–	–	–	–	–	–	–	–	–	–	–
	Seasonal average	**25.01**	**0.57**	**34.05**	**0.23**	**383.0**	**57.8**	**383.6**	**0.5**	**−0.5**	**57.8**	**0.5**	**9.7**	**10.26**	**0.04**	**1.10**
Spring	Mar. 1–5, 2004	–	–	–	–	–	–	–	–	–	–	–	–	–	–	–
	Mar. 20–31, 2009	25.86	0.35	33.94	0.09	357.5	3.9	375.6	0.3	−18.0	3.9	−2.8	1.0	7.40	0.05	1.25
	Apr. 29, 2004	–	–	–	–	–	–	–	–	–	–	–	–	–	–	–
	Apr. 10–25, 2005	–	–	–	–	–	–	–	–	–	–	–	–	–	–	–
	Apr. 20–30, 2008	27.67	0.29	33.90	0.08	379.0	8.2	372.8	0.2	6.2	8.2	0.6	0.4	6.17	0.04	1.21
	Apr. 1–21, 2009	26.25	0.30	33.79	0.09	369.4	2.8	374.4	0.6	−5.1	2.9	−1.0	2.0	8.60	0.05	1.20
	Apr. 30, 2011	–	–	–	–	–	–	–	–	–	–	–	–	–	–	–
	Apr. 9–29, 2012	–	–	–	–	–	–	–	–	–	–	–	–	–	–	–
	May 14–30, 2001	–	–	–	–	–	–	–	–	–	–	–	–	–	–	–
	May 1–28, 2004	–	–	–	–	–	–	–	–	–	–	–	–	–	–	–
	May 1–29, 2011	27.95	0.52	33.82	0.18	396.6	7.5	377.9	0.9	18.7	7.6	1.2	1.2	4.78	0.03	1.27
	May 23–31, 2014	30.83	0.36	33.85	0.19	441.2	7.0	379.8	0.2	63.3	7.0	3.5	0.1	4.31	0.03	1.30
	May 15–31, 2016	–	–	–	–	–	–	–	–	–	–	–	–	–	–	–
	Seasonal average	**27.71**	**0.37**	**33.86**	**0.14**	**388.7**	**6.2**	**376.1**	**0.5**	**13.0**	**6.3**	**0.3**	**1.2**	**6.25**	**0.04**	**1.25**
Summer	Jun. 2–3, 2001	–	–	–	–	–	–	–	–	–	–	–	–	–	–	–
	Jun. 1–20, 2014	29.51	0.36	33.54	0.18	407.2	9.1	380.7	0.4	26.5	9.1	2.9	1.2	6.33	0.04	1.19
	Jun. 1–5, 2016	–	–	–	–	–	–	–	–	–	–	–	–	–	–	–
	Jun. 5–27, 2017	–	–	–	–	–	–	–	–	–	–	–	–	–	–	–
	Jul. 10–21, 2000	–	–	–	–	–	–	–	–	–	–	–	–	–	–	–
	Jul 6–23, 2004	–	–	–	–	–	–	–	–	–	–	–	–	–	–	–
	Jul. 1–24, 2007	30.24	0.22	33.96	0.09	399.8	3.8	365.4	0.2	34.4	3.8	2.3	0.3	4.85	0.03	1.23
	Jul. 1–14, 2008	–	–	–	–	–	–	–	–	–	–	–	–	–	–	–
	Jul. 17–31, 2009	29.51	0.15	33.12	0.10	387.7	5.0	368.4	0.1	19.3	5.0	1.7	0.4	5.60	0.03	1.20
	Jul. 29–31, 2012	–	–	–	–	–	–	–	–	–	–	–	–	–	–	–
	Jul. 1–18, 2014	30.04	0.11	33.54	0.13	406.7	2.4	378.1	0.2	28.6	2.4	2.7	0.1	5.64	0.04	1.28
	Jul. 19–31, 2015	–	–	–	–	–	–	–	–	–	–	–	–	–	–	–
	Aug. 14–31, 2007	–	–	–	–	–	–	–	–	–	–	–	–	–	–	–
	Aug. 6–31, 2008	29.02	0.21	32.95	0.57	377.7	5.4	366.9	0.2	10.8	5.4	1.3	0.5	6.21	0.05	1.33
	Aug. 1–18, 2009	29.44	0.18	33.33	0.08	386.8	3.0	365.5	0.2	21.3	3.0	2.7	0.8	6.13	0.06	1.49
	Aug. 1–21, 2012	–	–	–	–	–	–	–	–	–	–	–	–	–	–	–
	Aug. 1–8, 2015	–	–	–	–	–	–	–	–	–	–	–	–	–	–	–
	Seasonal average	**29.63**	**0.22**	**33.41**	**0.26**	**394.3**	**5.2**	**370.8**	**0.2**	**23.5**	**5.2**	**2.2**	**0.7**	**5.79**	**0.04**	**1.29**
Fall	Sep. 18–30, 2004	28.87	0.20	33.69	0.17	359.7	1.7	355.3	0.2	4.5	1.7	0.5	0.4	6.59	0.03	1.11
	Sep. 30, 2006	–	–	–	–	–	–	–	–	–	–	–	–	–	–	–
	Sep. 1–14, 2007	–	–	–	–	–	–	–	–	–	–	–	–	–	–	–
	Oct. 10–24, 2003	–	–	–	–	–	–	–	–	–	–	–	–	–	–	–
	Oct. 1–2, 2004	–	–	–	–	–	–	–	–	–	–	–	–	–	–	–
	Oct. 1–6, 2006	–	–	–	–	–	–	–	–	–	–	–	–	–	–	–
	Oct. 25–31, 2010	–	–	–	–	–	–	–	–	–	–	–	–	–	–	–
	Nov. 11–16, 2002	–	–	–	–	–	–	–	–	–	–	–	–	–	–	–
	Nov. 25–30, 2006	–	–	–	–	–	–	–	–	–	–	–	–	–	–	–
	Nov. 1–26, 2010	–	–	–	–	–	–	–	–	–	–	–	–	–	–	–
	Seasonal average	**28.87**	**0.20**	**33.69**	**0.17**	**359.7**	**1.7**	**355.3**	**0.2**	**4.5**	**1.7**	**0.5**	**0.4**	**6.59**	**0.03**	**1.11**

Table 7
pCO_2, CO_2 fluxes and other parameters in Domain E during the surveys (Temp. is temperature; Atm. pCO_2 is atmospheric pCO_2).

Season	Survey period	Temp. (°C)		Salinity		Water pCO_2 (μatm)		Atm. pCO_2 (μatm)		ΔpCO_2 (μatm)		FCO_2 (mmol m^{-2} d^{-1})		Wind speed (m s^{-1})		C_2
		Mean	SD	Mean	SD	Mean	SD	Mean	SD	Mean	SD	Mean	SD	Mean	SD	Mean
Winter	Dec. 1–23, 2006	27.19	0.70	33.46	0.10	382.6	3.6	375.8	0.8	6.8	3.7	2.0	1.1	11.12	0.02	1.05
	Dec. 29–31, 2008	–	–	–	–	–	–	–	–	–	–	–	–	–	–	–
	Jan. 1–11, 2009	–	–	–	–	–	–	–	–	–	–	–	–	–	–	–
	Jan. 5–31, 2010	–	–	–	–	–	–	–	–	–	–	–	–	–	–	–
	Jan. 4–31, 2018	–	–	–	–	–	–	–	–	–	–	–	–	–	–	–
	Feb. 10–29, 2004	–	–	–	–	–	–	–	–	–	–	–	–	–	–	–
	Feb. 15–20, 2006	–	–	–	–	–	–	–	–	–	–	–	–	–	–	–
	Feb. 1–4, 2018	–	–	–	–	–	–	–	–	–	–	–	–	–	–	–
	Seasonal average	**27.19**	**0.70**	**33.46**	**0.10**	**382.6**	**3.6**	**375.8**	**0.8**	**6.8**	**3.7**	**2.0**	**1.1**	**11.12**	**0.02**	**1.05**
Spring	Mar. 1–5, 2004	–	–	–	–	–	–	–	–	–	–	–	–	–	–	–
	Mar. 20–31, 2009	–	–	–	–	–	–	–	–	–	–	–	–	–	–	–
	Apr. 29, 2004	29.02	0.15	33.88	0.08	393.1	2.5	363.2	0.2	29.9	2.5	1.5	0.2	4.32	0.01	1.16
	Apr. 10–25, 2005	28.43	0.21	33.94	0.09	409.5	8.6	369.4	0.2	40.1	8.6	3.0	0.7	5.39	0.02	1.14
	Apr. 20–30, 2008	–	–	–	–	–	–	–	–	–	–	–	–	–	–	–
	Apr. 1–21, 2009	–	–	–	–	–	–	–	–	–	–	–	–	–	–	–
	Apr. 30, 2011	–	–	–	–	–	–	–	–	–	–	–	–	–	–	–
	Apr. 9–29, 2012	–	–	–	–	–	–	–	–	–	–	–	–	–	–	–
	May 14–30, 2001	–	–	–	–	–	–	–	–	–	–	–	–	–	–	–
	May 1–28, 2004	29.59	0.18	33.84	0.05	388.0	3.5	362.8	0.2	25.2	3.5	1.9	0.4	5.27	0.02	1.18
	May 1–29, 2011	–	–	–	–	–	–	–	–	–	–	–	–	–	–	–
	May 23–31, 2014	–	–	–	–	–	–	–	–	–	–	–	–	–	–	–
	May 15–31, 2016	–	–	–	–	–	–	–	–	–	–	–	–	–	–	–
	Seasonal average	**29.01**	**0.18**	**33.89**	**0.08**	**396.9**	**5.5**	**365.1**	**0.2**	**31.7**	**5.5**	**2.1**	**0.5**	**4.99**	**0.02**	**1.16**
Summer	Jun. 2–3, 2001	–	–	–	–	–	–	–	–	–	–	–	–	–	–	–
	Jun. 1–20, 2014	–	–	–	–	–	–	–	–	–	–	–	–	–	–	–
	Jun. 1–5, 2016	–	–	–	–	–	–	–	–	–	–	–	–	–	–	–
	Jun. 5–27, 2017	29.93	0.10	33.44	0.06	417.4	2.1	389.3	0.1	28.1	2.1	2.8	0.2	6.31	0.01	1.09
	Jul. 10–21, 2000	–	–	–	–	–	–	–	–	–	–	–	–	–	–	–
	Jul 6–23, 2004	–	–	–	–	–	–	–	–	–	–	–	–	–	–	–
	Jul. 1–24, 2007	–	–	–	–	–	–	–	–	–	–	–	–	–	–	–
	Jul. 1–14, 2008	–	–	–	–	–	–	–	–	–	–	–	–	–	–	–
	Jul. 17–31, 2009	–	–	–	–	–	–	–	–	–	–	–	–	–	–	–
	Jul. 29–31, 2012	–	–	–	–	–	–	–	–	–	–	–	–	–	–	–
	Jul. 1–18, 2014	–	–	–	–	–	–	–	–	–	–	–	–	–	–	–
	Jul. 19–31, 2015	–	–	–	–	–	–	–	–	–	–	–	–	–	–	–
	Aug. 14–31, 2007	28.39	0.40	33.69	0.19	403.3	8.1	364.2	0.6	39.1	8.1	6.2	1.2	7.74	0.03	1.17
	Aug. 6–31, 2008	–	–	–	–	–	–	–	–	–	–	–	–	–	–	–
	Aug. 1–18, 2009	–	–	–	–	–	–	–	–	–	–	–	–	–	–	–
	Aug. 1–21, 2012	–	–	–	–	–	–	–	–	–	–	–	–	–	–	–
	Aug. 1–8, 2015	–	–	–	–	–	–	–	–	–	–	–	–	–	–	–
	Seasonal average	**29.16**	**0.29**	**33.57**	**0.14**	**410.4**	**5.9**	**376.8**	**0.4**	**33.6**	**5.9**	**4.5**	**0.9**	**7.0**	**0.02**	**1.13**
Fall	Sep. 18–30, 2004	–	–	–	–	–	–	–	–	–	–	–	–	–	–	–
	Sep. 30, 2006	–	–	–	–	–	–	–	–	–	–	–	–	–	–	–
	Sep. 1–14, 2007	29.20	0.37	32.84	0.44	403.4	7.8	363.1	0.3	40.3	7.8	3.5	0.7	5.54	0.02	1.25
	Oct. 10–24, 2003	–	–	–	–	–	–	–	–	–	–	–	–	–	–	–
	Oct. 1–2, 2004	–	–	–	–	–	–	–	–	–	–	–	–	–	–	–
	Oct. 1–6, 2006	–	–	–	–	–	–	–	–	–	–	–	–	–	–	–
	Oct. 25–31, 2010	–	–	–	–	–	–	–	–	–	–	–	–	–	–	–
	Nov. 11–16, 2002	–	–	–	–	–	–	–	–	–	–	–	–	–	–	–
	Nov. 25–30, 2006	–	–	–	–	–	–	–	–	–	–	–	–	–	–	–
	Nov. 1–26, 2010	–	–	–	–	–	–	–	–	–	–	–	–	–	–	–
	Seasonal average	**29.20**	**0.37**	**32.84**	**0.44**	**403.4**	**7.8**	**363.1**	**0.3**	**40.3**	**7.8**	**3.5**	**0.7**	**5.54**	**0.02**	**1.25**

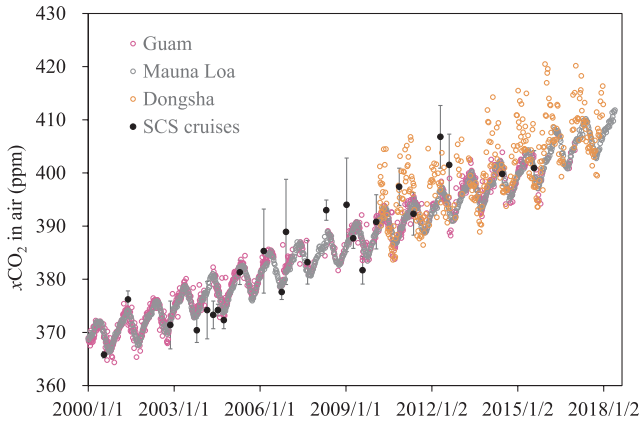

Fig. 5. Temporal distribution of atmospheric xCO_2 based on shipboard measurements during the cruises to the South China Sea (black dots with error bars) and time-series observations at Dongsha Island (orange dots) in the northern South China Sea, Guam (pink dots) in the North Pacific, and the Mauna Loa Observatory at Hawaii (grey dots). The error bars are the standard deviations. The stations at Dongsha Island and Guam are at 116.7297 °E, 20.6992 °N and 144.6560 °E, 13.3860 °N, respectively. Data at Dongsha Island and Guam are from the Earth System Research Laboratory, Global Monitoring Division, National Oceanic & Atmospheric Administration (http://www.esrl.noaa.gov/gmd/dv/site/). Data at Hawaii are from the Scripps CO_2 Program (http://scrippsco2.ucsd.edu/data). (For interpretation of the references to color in this figure legend, the reader is referred to the web version of this article.)

reduced to < 32, coinciding with relatively lower $NpCO_2$ values (Fig. 9C-2). In summary, pCO_2 in Domain C was primarily dominated by seasonal variations in SST. pCO_2 in Domain D was influenced by the Pearl River plume in summer (the northwestern corner) and enhanced vertical mixing induced by upwelling in winter, in addition to SST variations. Domain E was influenced by the Mekong River plume in addition to SST variations.

4.5. Air-sea CO_2 fluxes

4.5.1. Intra-seasonal variations

Among the cruise observations, significant intra-seasonal changes occurred, which could affect the overall carbon budgeting over a longer seasonal and/or annual time-scale.

The NSCS (> 18°N) was generally a CO_2 sink in winter except in Domain D, and a CO_2 source in summer, while spring and fall were transitional periods from a sink to a source and from a source to a sink, respectively. In winter, although Domains A and B were CO_2 sinks, Domain D showed intra-seasonal variability. For Domain D, we have only three winter cruises. ΔpCO_2 in December 2006 (15.4 µatm), when strong upwelling was observed, was much higher than in January of 2010 (4.7 µatm) and 2018 (-21.6 µatm), when upwelling was much weaker. As a consequence, the CO_2 source in December 2006 (4.4 mmol m^{-2} d^{-1}) was larger than in January 2010 (1.1 mmol m^{-2} d^{-1}). January 2018 was even a CO_2 sink (CO_2 flux of −4.0 mmol m^{-2} d^{-1}). Although wind speed had a strong influence on the calculated CO_2 fluxes, its impact on intra-seasonal CO_2 flux variability was secondary compared to the effect of ΔpCO_2. In Domains C and E, we have only one winter cruise in each domain, and thus no intra-seasonal variations can be discussed.

In spring, Domain A was generally a CO_2 sink (CO_2 fluxes of −2.2 to −6.1 mmol m^{-2} d^{-1}), but it was a weak source of 0.2–0.3 mmol m^{-2} d^{-1} in May of 2011 and 2016. This was due primarily to positive ΔpCO_2 values (4.1 and 4.6 µatm) compared to the negative ΔpCO_2 values observed during the other cruises (–22.4 to −44.1 µatm). The positive

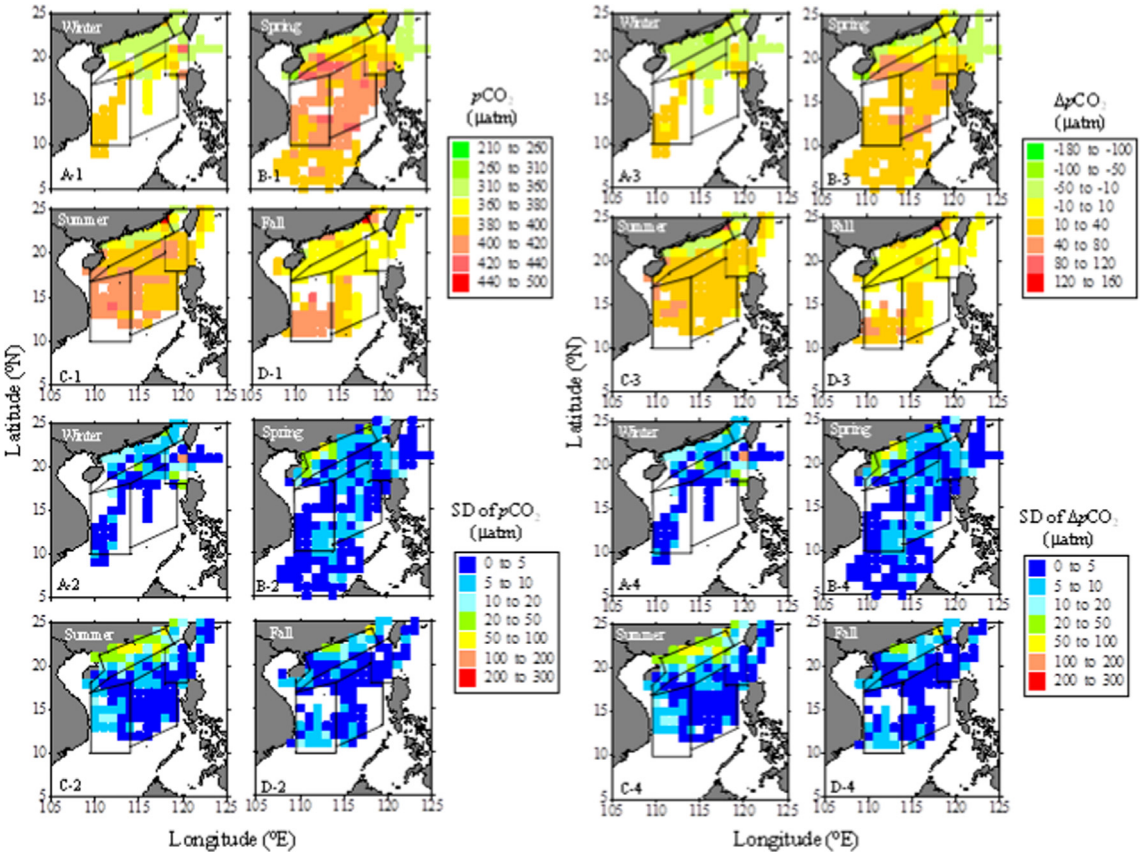

Fig. 6. Distribution of seasonal averages and standard deviations (SD) of pCO_2 and ΔpCO_2 in 1°×1° grids in the South China Sea. The pCO_2 values were normalized to the year 2010.

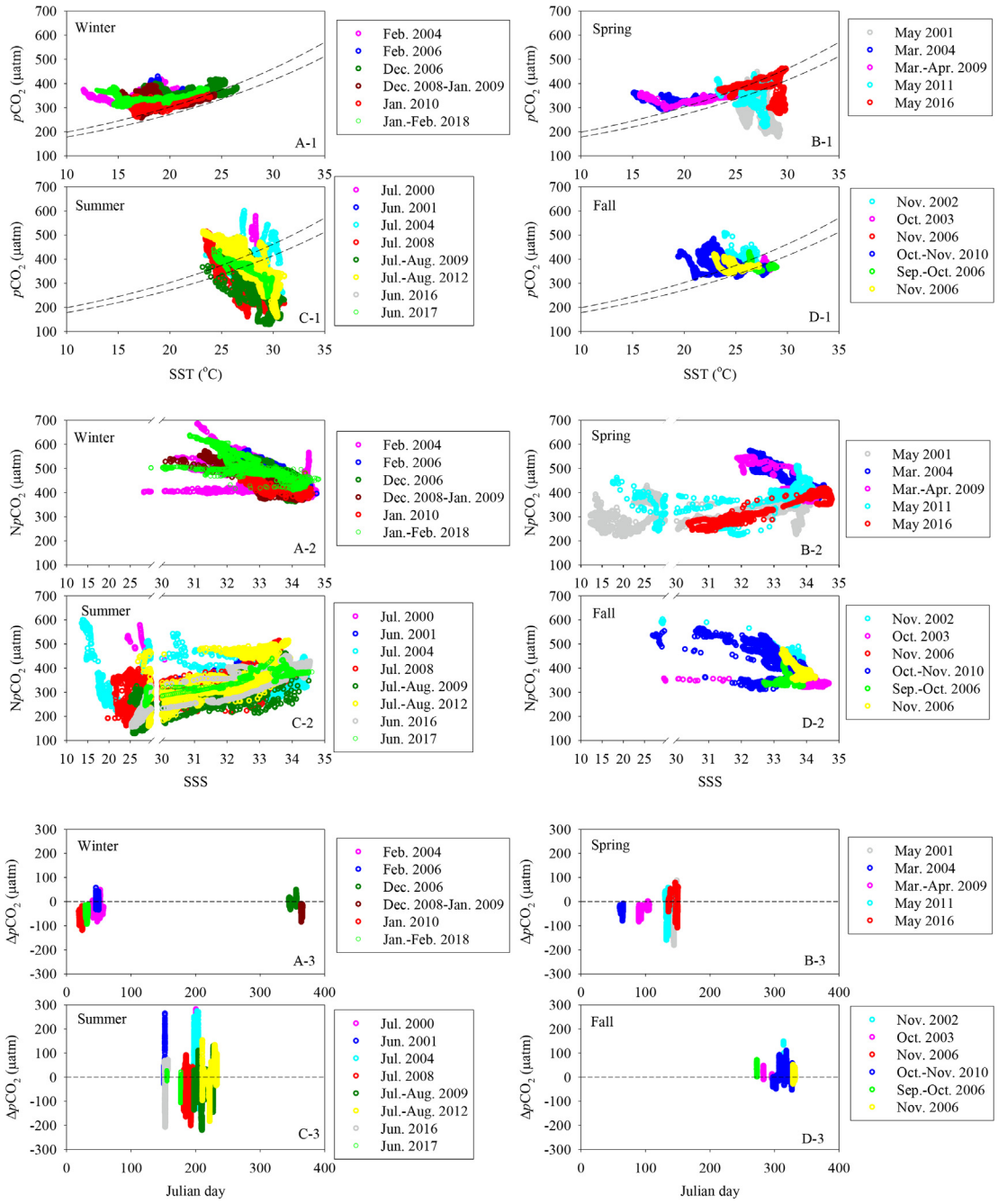

Fig. 7. Relationships of surface water pCO_2 and sea surface temperature (SST), as well as normalized pCO_2 to 26 °C ($NpCO_2$) and sea surface salinity (SSS) in Domain A. pCO_2 values are for the noted year of observations. The dashed lines in panels A-1 to D-1 show the SST-dominated pCO_2 range ($350 \times e^{0.0423(SST-26)}$ and $390 \times e^{0.0423(SST-26)}$) according to Zhai et al. (2013).

ΔpCO_2 values (and higher seawater pCO_2) observed during the May cruises might be due to the much higher SSTs (> 27 °C) compared to March and April (< 25 °C). In Domain B, spring was a transitional period from a CO_2 sink to a CO_2 source. In March of 2004 and April of 2009, when the domain was a CO_2 sink (CO_2 fluxes of −1.0 to −1.9 mmol m^{-2} d^{-1}), the SST (< 26 °C) was much lower than during the other spring cruises (SST > 27 °C) when it was a CO_2 source (1.6–4.5 mmol m^{-2} d^{-1}, Table 4). The intra-seasonal variability of CO_2 fluxes in Domain D was similar to that of Domain B and it was likely controlled by SST. Domain D was a CO_2 sink in March and April when the SST was < 27 °C and a CO_2 source in May when the SST was > 27 °C (Table 6, Fig. 10). Domains C and E were CO_2 sources of 1.4–3.0 mmol m^{-2} d^{-1} during all spring cruises, and intra-seasonal variations were relatively smaller.

In summer, pCO_2 in Domain A was primarily influenced by the Pearl River plume, coastal upwelling and the high SST as stated above; the Pearl River plume was a moderate CO_2 sink but the area beyond the plume was a moderate CO_2 source. Although Domains B, C, D and E were all CO_2 sources, the intra-seasonal flux variations in Domains B and D were larger than those of Domains C and E. The range of the calculated CO_2 fluxes in Domain D was 1.3–2.9 mmol m^{-2} d^{-1}, which was primarily attributed to the intra-seasonal variability of both ΔpCO_2 and wind speed. The intra-seasonal variations of CO_2 fluxes in Domains C and E were rather small (2.0–2.8 mmol m^{-2} d^{-1}), except during the August 2007 cruise when a cold-core eddy was observed. The small intra-seasonal variations in these two domains were attributed to both

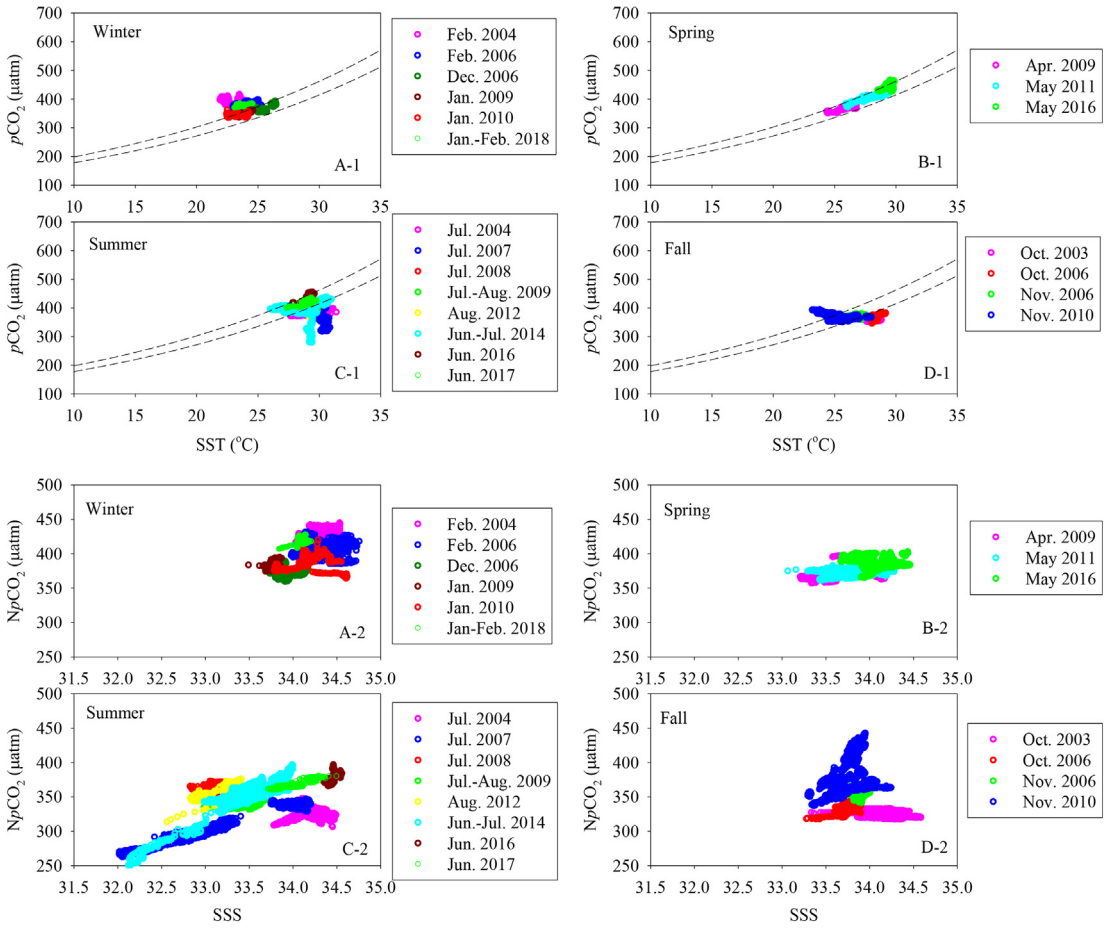

Fig. 8. Relationships of surface water pCO_2 and sea surface temperature (SST), as well as normalized pCO_2 to 26 °C ($NpCO_2$) and sea surface salinity (SSS) in Domain B. pCO_2 values are for the noted year of observations. The dashed lines in panels A-1 to D-1 show the SST-dominated pCO_2 range ($350 \times e^{0.0423(SST-26)}$ and $390 \times e^{0.0423(SST-26)}$) according to Zhai et al. (2013).

the stable ΔpCO_2 values and wind speeds (variation < 20% among the cruises). During the August 2007 cruise (cold-core eddy observed), the high CO_2 flux in Domain E (6.2 mmol m^{-2} d^{-1}) was due to the combined effect of the highest ΔpCO_2 (39.1 μatm) and wind speed (7.74 m s^{-1}) among the summer cruises (Table 7).

In fall, Domain A ranged from a strong source to a moderate sink of CO_2 (CO_2 fluxes of −2.6 to 8.2 mmol m^{-2} d^{-1}), and Domain B from a weak source to a moderate sink (CO_2 fluxes of 0.9 to −2.0 mmol m^{-2} d^{-1}, Tables 3 and 4). In Domains A and B, seawater pCO_2 was generally higher than atmospheric pCO_2 in September and October, but decreased to lower than atmospheric pCO_2 in November. Nevertheless, the controlling factors in Domain A were more complex. For example, the high water pCO_2 observed in November 2002 (Table 3) might be the result of a winter monsoon burst delay in that year (Zhai et al., 2005). Excluding this cruise, the NSCS was generally a CO_2 source in September and a CO_2 sink in November, while October acted as a transitional period from a source to a sink (Fig. 11). Domains C, D and E were all CO_2 sources in fall based on the surveys, but data were too limited to discuss intra-seasonal variations.

In summary, Domains A, B and D showed large intra-seasonal variations, especially in spring and fall. In addition to the influence of the Pearl River plume, the intra-seasonal variability of CO_2 fluxes might be primarily due to variations in SST. Spring was a transitional season from a CO_2 sink (March) to a CO_2 source (May), and fall was a transitional season from a CO_2 source (September) to a CO_2 sink (November). In summer, the domains were CO_2 sinks in the area of the Pearl River plume and CO_2 sources in the areas beyond the plume. In winter, although Domains A and B were CO_2 sinks, Domain D was either a CO_2 source or sink depending on the level of upwelling; it was a strong source during periods of intense upwelling and a weak source or even a sink during periods of reduced upwelling. Domain D in summer was a CO_2 source with weak intra-seasonal variability due to the smaller intra-seasonal variations in both ΔpCO_2 and wind speed. Domains C and E were CO_2 sources with weak intra-seasonal variability in spring and summer due primarily to the smaller intra-seasonal variations in ΔpCO_2 and wind speed. In addition to the high SST in all seasons, the general CO_2 sources in Domains C and E were likely related to the deep water input from the adjacent northwestern Pacific and the stronger vertical mixing in the SCS basin as suggested by Dai et al. (2013).

4.5.2. Seasonal and annual CO_2 fluxes

With the five domains categorized, we observed overall well-defined seasonality in CO_2 fluxes in the individual domains.

Air-sea CO_2 fluxes showed strong seasonal variability in each domain, and the seasonal pattern differed among the domains (Tables 3 to 7 and Fig. 10). Generally, Domain A was a moderate to strong CO_2 sink in winter (CO_2 fluxes of −1.3 to −11.8 mmol m^{-2} d^{-1}), a strong sink to in near equilibrium with the atmosphere in spring (CO_2 fluxes of −6.1 to 0.3 mmol m^{-2} d^{-1}), in near equilibrium with the atmosphere in summer (CO_2 fluxes of −0.2 ± 4.4 mmol m^{-2} d^{-1}) and a weak source in fall (1.2 ± 2.8 mmol m^{-2} d^{-1}). Domain B was a moderate sink in winter (CO_2 fluxes of −3.8 ± 2.1 mmol m^{-2} d^{-1}), a moderate sink to a moderate source in spring (CO_2 fluxes of −1.9 to 4.5 mmol m^{-2} d^{-1}), a moderate source in summer (1.9–3.8 mmol m^{-2} d^{-1}) and in near equilibrium with the atmosphere in fall (-0.7 to

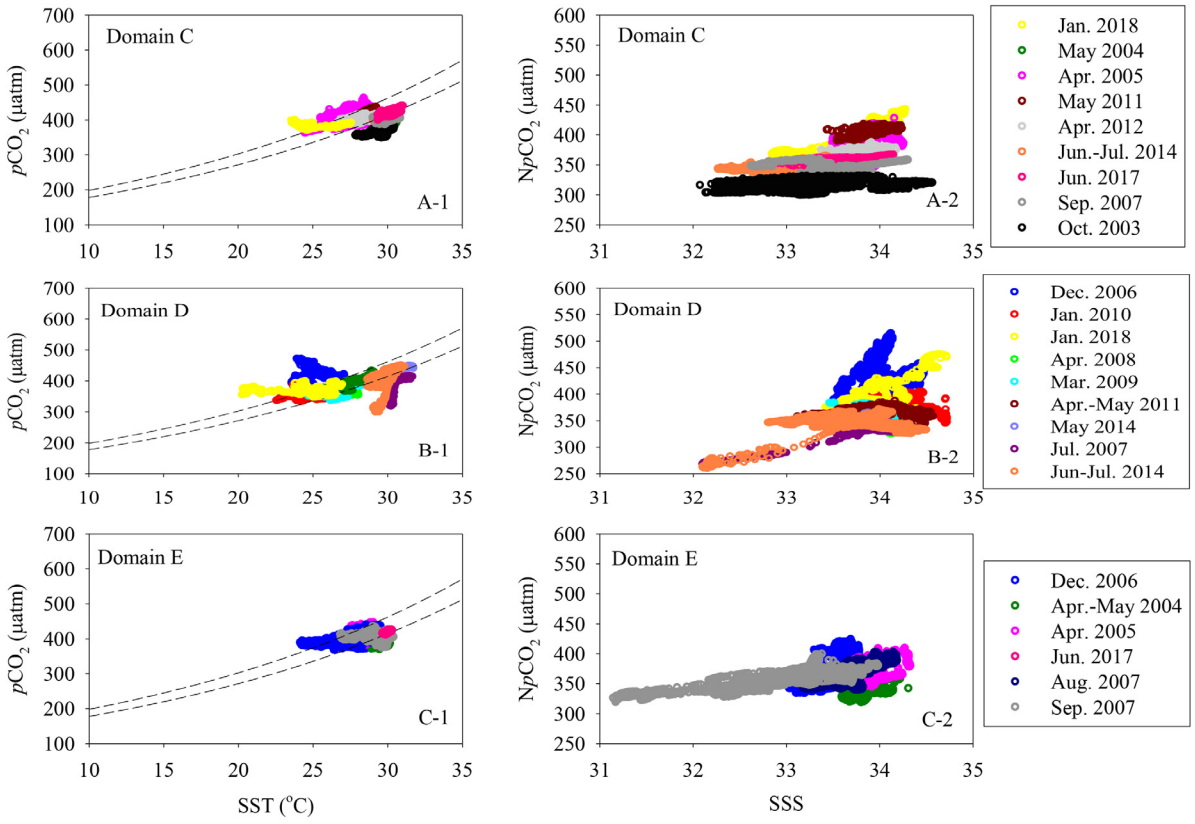

Fig. 9. Relationships of surface water pCO_2 and sea surface temperature (SST), as well as normalized pCO_2 to 26 °C ($NpCO_2$) and sea surface salinity (SSS) in Domains C, D and E. pCO_2 values are for the noted year of observations. The dashed lines in panels A-1 to C-1 show the SST-dominated pCO_2 range ($350 \times e^{0.0423(SST-26)}$ and $390 \times e^{0.0423(SST-26)}$) according to Zhai et al. (2013).

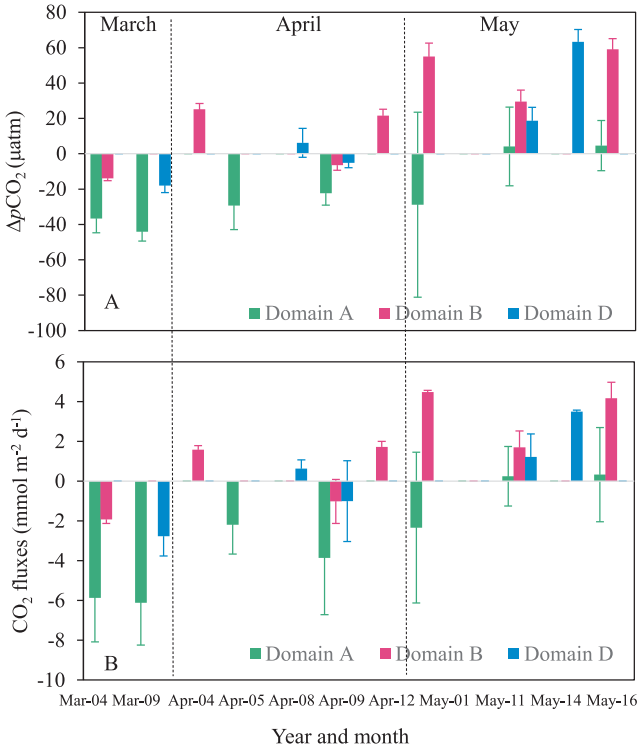

Fig. 10. ΔpCO_2 and air-sea CO_2 fluxes in the northern SCS in Domains A, B and D in spring. The error bars are the standard deviations. Each bar is a cruise or leg in the specified season. The x-axis is year and month in the format of mmm-yy. The vertical dashed lines separate the months.

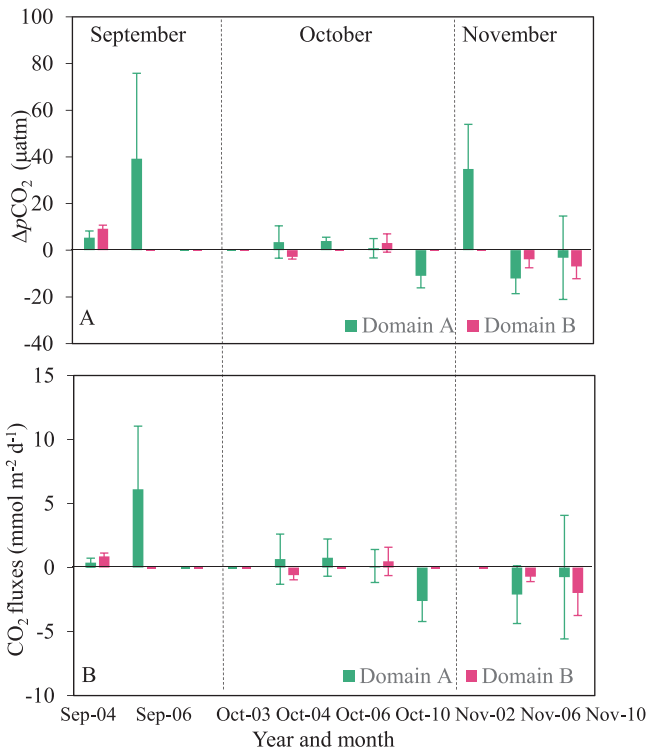

Fig. 11. ΔpCO_2 and air-sea CO_2 fluxes in the northern SCS in Domains A and B in fall. The error bars are the standard deviations. Each bar is a cruise or leg in the specified season. The x-axis is year and month in the format of mmm-yy. The vertical dashed lines separate the months.

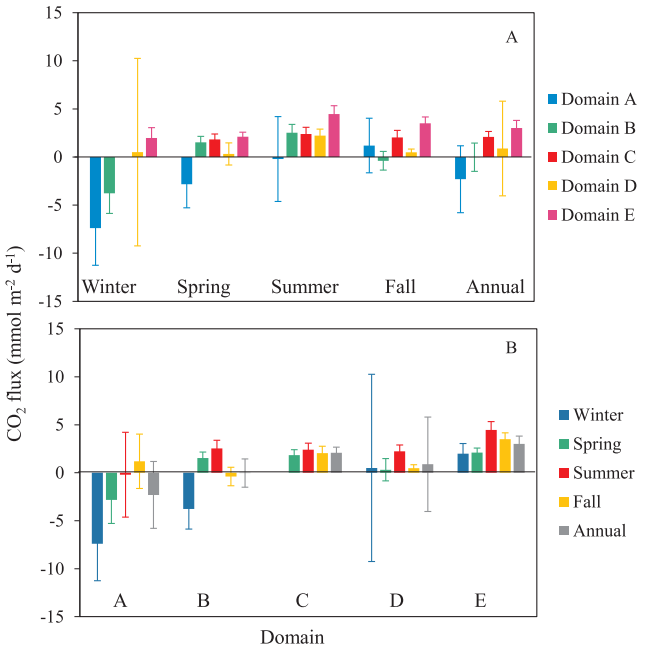

Fig. 12. CO_2 fluxes and seasonal variations in the SCS. The error bars are the standard deviations.

0.9 mmol m^{-2} d^{-1}) except in November 2010 (Table 4). Domain C was a weak to moderate source from spring to fall (1.2–2.8 mmol m^{-2} d^{-1}). Domain D ranged from a moderate sink to a moderate source in winter and spring (CO_2 fluxes of −4.0 to 4.4 mmol m^{-2} d^{-1}) and a weak to moderate source in summer and fall (CO_2 fluxes of 0.5–2.9 mmol m^{-2} d^{-1}). Domain E was a moderate to strong source all year round with a flux range of 1.5–6.2 mmol m^{-2} d^{-1}.

Seasonally, Domain A was a CO_2 sink in winter and spring, in near equilibrium with the atmosphere in summer and a CO_2 source in fall. Domain B was a CO_2 sink in winter, a CO_2 source in spring and summer and in near equilibrium with the atmosphere in fall. Domains C, D and E were CO_2 sources during all seasons (Fig. 12). Annually, Domain A was a sink of 2.3 ± 3.5 mmol m^{-2} d^{-1}; Domain B was in near equilibrium with the atmosphere; and Domains C, D and E were CO_2 sources of 0.9–3.0 mmol m^{-2} d^{-1}. For the 5 domains, the area-weighted CO_2 flux was −1.1 ± 2.2 mmol m^{-2} d^{-1} in winter, 0.9 ± 0.9 mmol m^{-2} d^{-1} in spring, 2.5 ± 1.4 mmol m^{-2} d^{-1} in summer and 1.9 ± 1.1 mmol m^{-2} d^{-1} in fall. The annual average CO_2 flux was 1.2 ± 1.7 mmol m^{-2} d^{-1}.

It should be noted that the CO_2 flux data in winter from Domain C was excluded from the calculation of the annual average, as there was only one winter cruise and the surveyed area covered < 1/3 of the domain's surface area. During that winter cruise, Domain C acted as a sink of atmospheric CO_2. If more investigations in the future support that the basin is a CO_2 sink in winter, the above estimate of the annual source from the SCS would be an overestimate.

The SEATS time-series station is located in the north of Domain C and close to Domain B. As Domain C covers a very large latitudinal range, we compare the results in the literature from SEATS with our results from Domain B. Tseng et al. (2007) reported that the NSCS at SEATS acts as a CO_2 source during warm seasons and a CO_2 sink during cold seasons, with a CO_2 flux range from ~−4 to 5 mmol m^{-2} d^{-1} and an annual average flux of −0.05 mmol m^{-2} d^{-1} based on seasonal observations from 1999-2004. Sheu et al. (2010) reported the air-sea CO_2 flux at SEATS to range from ~−3 to 3 mmol m^{-2} d^{-1} with an annual average flux of 0.6 mmol m^{-2} d^{-1} based on seasonal observations from 1999 to 2009. The air-sea CO_2 fluxes, seasonal flux variations and the annual average CO_2 flux (0.0 ± 1.5 mmol m^{-2} d^{-1}) we estimated for Domain B are comparable to those of Tseng et al. (2007) and Sheu et al. (2010). Our finding of the SCS basin as a CO_2 source during the wet season and a CO_2 sink during the dry season is comparable with previous findings by Chen et al. (2006). Additionally, the estimated CO_2 fluxes in fall in this study are comparable to those in Xu et al. (2016).

The surface area of the 5 domains is 1.35 × 10^6 km^2. The average annual CO_2 emission from the 5 domains over the study period was 7.2 ± 10.0 Tg C yr^{-1}. Extrapolating to the entire SCS proper (2.5 × 10^6 km^2 excluding the Gulf of Thailand and Gulf of Tonkin), the SCS emitted 13.3 Tg C yr^{-1} of CO_2. This value is ~ 40% of that determined by Zhai et al. (2013). There are likely several probable reasons for this "inconsistency". Although the categorization of domains in this study was different from that of Zhai et al. (2013), our Domains A, B and D were in similar locations as in Zhai et al. (2013), and therefore we can compare the three domains directly. Also, because our Domains C and E were in a similar location as the Domain C of Zhai et al. (2013), we compare the area-weighted values of our Domains C and E with those of their Domain C.

Firstly, comparing our flux estimates to Zhai et al. (2013), after 2007 the CO_2 sink we observed in Domains A and B in winter was stronger, but the CO_2 source we observed in Domain D was weaker. In Domains A and B, our study integrated the data collected from 8 winter surveys from 2004 to 2018, while Zhai et al. (2013) complied only 3 winter surveys (February 2004, February 2006 and December 2006). The CO_2 sink in Domains A and B in winter after 2007 doubled or even tripled compared to before 2007 (Table 3 and Fig. 13). Domain D in winter was found to be a weaker CO_2 source when more data were integrated as compared to the strong source reported by Zhai et al. (2013). In Zhai et al. (2013), there was only one winter survey (December 2006) when the CO_2 source was strong; in this study we compiled data collected from 2 additional surveys (January of 2010 and 2018). During the December 2006 cruise (the only winter cruise of Zhai et al. (2013)), strong upwelling induced a CO_2 source of 4.4 ± 7.2 mmol m^{-2} d^{-1}. However, during the January 2010 and January 2018 cruises, the upwelling was weaker and Domain D was a weak CO_2 source or even a CO_2 sink (CO_2 fluxes of 1.1 and −4.0 mmol m^{-2} d^{-1}). Therefore, the average estimated CO_2 flux to the

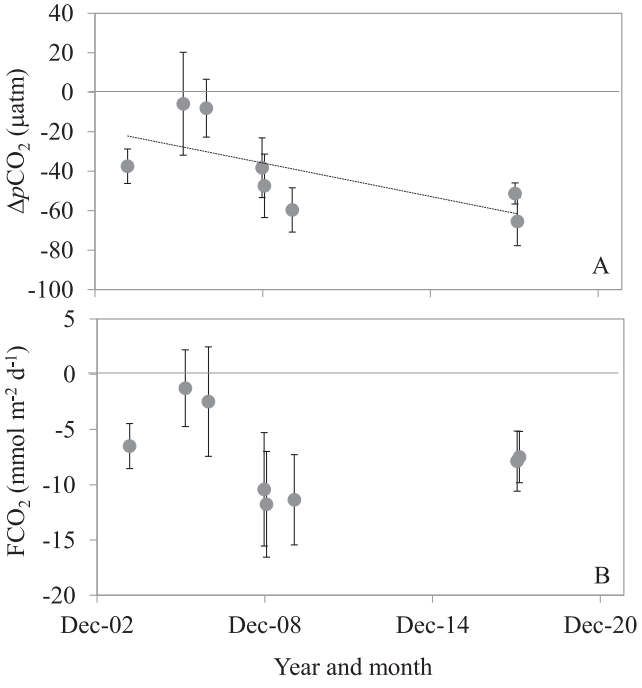

Fig. 13. ΔpCO_2 and air-sea CO_2 fluxes in Domain A in winter. The error bars are the standard deviations. The dashed line in panel A is the trendline. X-axis is year and month in the format of mmm-yy.

atmosphere from Domain D in winter in this study was only 16% of that found by Zhai et al. (2013). Additionally, the ratios of surface area of Domains A and B to total study area in this study (29%) were larger than those in Zhai et al. (2013) (21%), which also lowered the CO_2 source estimate when extrapolated to the entire SCS. The above variation in CO_2 fluxes and area ratios "converted" the SCS in winter from a CO_2 source (CO_2 flux of 3.1 ± 2.3 mmol m^{-2} d^{-1}) in Zhai et al. (2013) to a CO_2 sink (-1.1 ± 2.2 mmol m^{-2} d^{-1}) in this study.

Secondly, we compiled data collected from 10 additional spring surveys, which resulted in a much weaker CO_2 source estimate in spring compared to that in Zhai et al. (2013). In our study, Domain A during most cruises was a CO_2 sink, which resulted in the annual average negative CO_2 flux of this domain (CO_2 flux of −2.8 ± 2.5 mmol m^{-2} d^{-1}, Table 3), rather than a CO_2 source as reported by Zhai et al. (2013) based on data from 3 cruises. In Domains C and E, we compiled a larger set of cruise data and the positive CO_2 fluxes we observed were lower than those observed during the cruises adopted by Zhai et al. (2013). These discrepancies in cruise data resulted in the estimated CO_2 source in this study being only ~ 40% of that reported by Zhai et al. (2013).

Thirdly, the estimated CO_2 source from Domains C and E (accounting for 62% of the total surface area of the 5 domains) in summer was much smaller in this study. Zhai et al. (2013) estimated the CO_2 flux from the SCS basin (their Domain C) in summer based on only 1 summer cruise (August 2007 when cold-core eddy was observed), while here we compiled data from 5 summer surveys in our Domain C and 2 surveys in our Domain E. Among the summer cruises, the CO_2 flux in August 2007 (the only summer cruise in Zhai et al. (2013)) was 2.2 times that of the multi-cruise average values. This resulted in the fact that the estimated area-weighted CO_2 source in summer in this study was only 58% of that reported by Zhai et al. (2013).

In fall, the data in Domains C, D and E we adopted are the same as those of Zhai et al. (2013), so the area-weighted CO_2 fluxes we estimated for these three domains are very similar to those of Zhai et al. (2013). With the inclusion of data after 2009, Domain A became a stronger CO_2 source but Domain B became a weak sink from a source. The overall CO_2 source we estimated was ~ 70% of that in Zhai et al. (2013). Additionally, for the data collected from the same cruise that both we and Zhai et al. (2013) adopted, the different categorization of domains and the wind speed data might also have resulted in differences in CO_2 flux estimations for each domain.

It should be noted that the large error bars in this study mostly reflect the temporal and spatial variations rather than the bulk uncertainties, the latter of which include the analytical error, the spatial variance, and the bias from undersampling (Wang et al., 2014). Decomposing the uncertainties is promising to better constrain the air-sea CO_2 fluxes for further study.

According to our air-sea CO_2 flux study in the SCS and comparison with the literature, high-frequency observations across the different seasons and areas that have large variability and/or a poor understanding of the carbon cycle are needed to reduce the uncertainties from undersampling and to further improve estimates of CO_2 fluxes. Ideally, multidimensional observations, including buoy-based time-series, ship-based surveys and remote sensing are promising to better constrain the air-sea CO_2 fluxes in the large, dynamic marginal seas.

Compared with other marginal seas, the CO_2 source level in the SCS is similar to that of the Ecuador-Chile coast (1.6 mmol m^{-2} d^{-1}) and the Weddell Sea (1.9 mmol m^{-2} d^{-1}) (Stoll et al., 2002, Torres et al., 2011, Torres et al., 2003), but lower than the western Arabian sea shelf (Sarma et al., 1998, Sarma et al., 2003) or the western Florida shelf (Cai et al., 2006), and much lower than the upwelling systems such as the southern Bering Sea slope (Fransson et al., 2006), the central California upwelling region (Friederich et al., 2002), or the Peru coast (Friederich et al., 2008). The weak CO_2 source of the SCS is consistent with the weak source or sink pattern of the low latitude marginal seas in the northern hemisphere (Laruelle et al., 2014). However, the CO_2 source of the SCS is lower than the low latitude western boundary ocean margins (Cai et al., 2006, Dai et al., 2013).

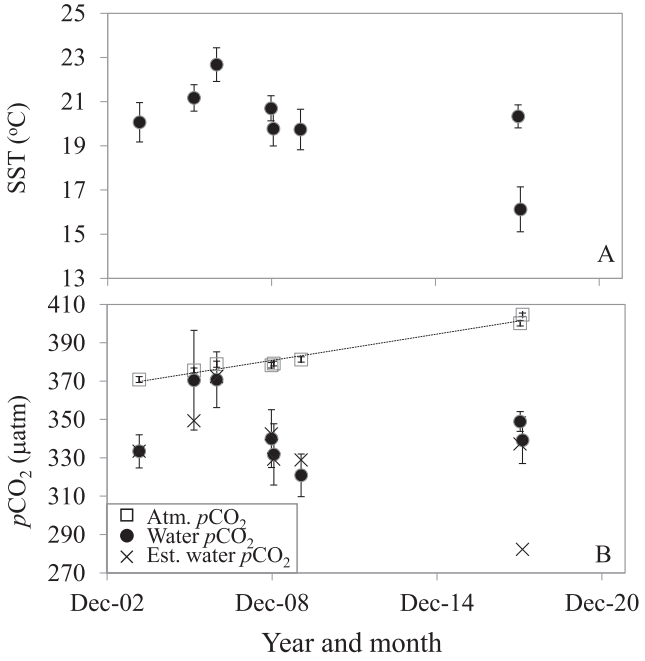

Fig. 14. Variations of SST, water pCO_2 and atmospheric pCO_2 (Atm. pCO_2) in Domain A in winter. The error bars are the standard deviations. The gray crosses are the estimated thermodynamic water pCO_2 (Est. water pCO_2) values based on the SST and water pCO_2 according to Takahashi et al. (1993). The dashed line is the linear regression line of the atmospheric pCO_2. X-axis is year and month in the format of mmm-yy.

4.5.3. The enhanced CO_2 sink on the NSCS shelf in winter

In winter, although Domain A was generally a sink area of atmospheric CO_2, we observed inter-annual variations. ΔpCO_2 and CO_2 fluxes showed a trend of increasing sink from February 2006 (Fig. 13). The average ΔpCO_2 and CO_2 fluxes in 2004–2006 were −17.1 ± 18.0 µatm and −3.4 ± 3.7 mmol m^{-2} d^{-1}, respectively, and changed to −52.4 ± 12.6 µatm and −9.8 ± 4.0 mmol m^{-2} d^{-1} in 2007–2018. This trend was consistent with the enhanced CO_2 sink in the global marginal seas reported by Laruelle et al. (2018).

SST in winter in Domain A showed an increasing (from 20 °C to 22.7 °C) and then decreasing (to 16–20 °C) pattern since 2004 (Fig. 14A). Seawater pCO_2 showed a similar trend as SST except in February 2018 (Fig. 14B). We estimated the thermodynamic surface water pCO_2 based on the pCO_2 and SST in February 2004 according to Takahashi et al. (1993); pCO_2 increases or decreases with SST at a coefficient of 4.23% $°C^{-1}$. The estimated water pCO_2 values showed a similar pattern to measured pCO_2 values except in February 2018 (Fig. 14B). For example, the SST during the December 2006 cruise was 2.6 °C higher than during February 2004. An increase of 2.6 °C would result in a 38.9 µatm increase in pCO_2 to 372.3 µarm, which was consistent with the observed pCO_2 (370.8 µatm). For the February 2018 cruise, the surveyed area was the very shallow coast (Fig. 2C), due to the influence of very rough seas which might have resulted in enhanced vertical mixing of CO_2-replete subsurface or bottom water and much higher pCO_2 values than estimated thermodynamically (Fig. 14B).

Atmospheric pCO_2 generally increased, showing a significant linear increase of 2.6 µatm yr^{-1} from 2004 to 2018 during the winter cruises ($n = 8$, $R^2 = 0.97$, $p < 0.0001$, Fig. 14B). This was similar to the rate of increase of atmospheric xCO_2 values of 2.2 ppm yr^{-1} based on time-series data on Dong-Sha Island from 2010 and 2017. However, water pCO_2 did not show a general trend (Fig. 14B). Therefore, the enhanced negative ΔpCO_2 in Domain A was primarily dominated by the lagging increase in water pCO_2 as compared to the atmospheric pCO_2,

consistent with other margins as suggested by Laruelle et al. (2018).

For the calculated air-sea CO_2 fluxes, wind speed and C_2 also played an important role. Although these parameters substantially affected air-sea CO_2 exchanges, the enhanced negative ΔpCO_2 likely dominated the intensified wintertime CO_2 sink on the NSCS shelf.

5. Concluding remarks

Based on the data collected from 47 surveys in the SCS from 2000 to 2018, surface water pCO_2 and associated air-sea CO_2 fluxes are robustly defined. Both pCO_2 and CO_2 fluxes in the SCS show strong temporal and spatial variations. The NSCS shelf is a moderate to strong CO_2 sink in winter and a weak sink in summer. However, transitional periods occur with the region changing from a sink to a source in spring and from a source to a sink in fall. Different from the NSCS, the WSCS is a moderate CO_2 source in all seasons. The SCS basin is also a CO_2 source except in winter. The major controls on pCO_2 differ across the different domains. pCO_2 in the NSCS is primarily dominated by biological CO_2 uptake and warming in spring and summer, ventilation in fall, and vertical mixing and cooling in winter. pCO_2 in the WSCS is dominated by temperature, with high SSTs inducing high pCO_2 over the entire year. On an annual basis, the entire SCS is a CO_2 source of 1.2 ($\pm$ 1.7) mmol m^{-2} d^{-1} and it releases 13.3 Tg C to the atmosphere annually based on our observations from 2000 to 2018. Consistent with the pattern of the global marginal seas, the CO_2 sink in winter on the NSCS shelf is increasing. Compared to the low latitude western boundary marginal seas, the SCS is a smaller CO_2 source. The annual average CO_2 flux was significantly lower than the previous estimate, which can largely be attributed to the addition of new datasets covering previously under-sampled seasons and regions. It is applicable to other complex and highly variable ocean margin environments around the world, and it is a great piece of evidence in support of continued frequent sampling in these coastal environments.

Declaration of Competing Interest

The authors declare that the study was conducted in the absence of any commercial or financial relationships that could be construed as a potential conflict of interest.

Acknowledgements

Baoshan Chen, Yuancheng Su, Yan Li, Jinwen Liu, Zhimian Cao, Gui Chen, and Yi Wang are appreciated for data collection during some of the cruises. Dr. Xianqiang He at the Second Institute of Oceanography (MNR) processed the remote sensing wind speed and SST data; Guoqiang Qiu at Xiamen University processed the remote sensing chlorophyll a data. This study was jointly supported by the Ministry of Science and Technology of the People's Republic of China through National Basic Research Program (2015CB954001, CHOICE-C II), the National Natural Science Foundation of China (#4173000226) and the State Oceanic Administration of China through grant GASI-03-01-02-02. We are grateful to the crews and technical staffs of the R/V Dongfanghong 2, Jiageng (TKK), Yanping 2, Shiyan 3, Haidiao 6, Haijian 83, and the Kexue 3 for their help during the cruises. We also appreciate the constructive comments and suggestions from two anonymous reviewers, which have improved the quality of this paper.

Appendix A. Supplementary material

Supplementary data to this article can be found online at https://doi.org/10.1016/j.pocean.2020.102272.

References

Borges, A.V., Delille, B., Frankignoulle, M., 2005. Budgeting sinks and sources of CO_2 in the coastal ocean: diversity of ecosystems counts. Geophys. Res. Lett. 32 (14), 14601 doi:14610.11029/12005GL023053.

Cai, W.-J., Dai, M.H., Wang, Y.C., 2006. Air-sea exchange of carbon dioxide in ocean margins: a province-based synthesis. Geophys. Res. Lett. 33 (12). https://doi.org/10.1029/2006GL026219.

Cao, Z.M., Dai, M.H., Zheng, N., Wang, D.L., Li, Q., Zhai, W.D., Meng, F.F., Gan, J.P., 2011. Dynamics of the carbonate system in a large continental shelf system under the influence of both a river plume and coastal upwelling. J. Geophys. Res.-Biogeosci. 116, G02010 doi:02010.01029/02010JG001596.

Caruso, M.J., Gawarkiewicz, G.G., Beardsley, R.C., 2006. Interannual variability of the Kuroshio intrusion in the South China Sea. J. Oceanogr. 62 (4), 559–575.

Chao, S.Y., Shaw, P.T., Wu, S.Y., 1996. El Nino modulation of the South China Sea circulation. Prog. Oceanogr. 38 (1), 51–93.

Chen, C.T.A., Borges, A.V., 2009. Reconciling opposing views on carbon cycling in the coastal ocean: Continental shelves as sinks and near-shore ecosystems as sources of atmospheric CO_2. Deep-Sea Res. II 56 (8–10), 578–590.

Chen, C.T.A., Huang, T.H., Chen, Y.C., Bai, Y., He, X., Kang, Y., 2013. Air-sea exchanges of CO_2 in the world's coastal seas. Biogeosciences 10 (10), 6509–6544.

Chen, C.T.A., Wang, S.L., Chou, W.C., Sheu, D.D., 2006. Carbonate chemistry and projected future changes in pH and $CaCO_3$ saturation state of the South China Sea. Mar. Chem. 101 (3–4), 277–305.

Chen, C.T.A., Wang, S.L., Wang, B.J., Pai, S.C., 2001. Nutrient budgets for the South China Sea basin. Mar. Chem. 75 (4), 281–300.

Chen, W.F., Liu, Q., Huh, C.A., Dai, M.H., Miao, Y.C., 2010. Signature of the Mekong River plume in the western South China Sea revealed by radium isotopes. J. Geophys. Res.-Oceans 115, C12002 doi:12010.11029/12010JC006460.

Chen, Y.L.L., 2005. Spatial and seasonal variations of nitrate-based new production and primary production in the South China Sea. Deep-Sea Res. I 52 (2), 319–340.

Chou, W.C., Sheu, D.D.D., Chen, C.T.A., Wang, S.L., Tseng, C.M., 2005. Seasonal variability of carbon chemistry at the SEATS time-series site, northern South China Sea between 2002 and 2003. Terrestrial Atmos. Oceanic Sci. 16 (2), 445–465.

Dai, M., Cao, Z., Guo, X., Zhai, W., Liu, Z., Yin, Z., Xu, Y., Gan, J., Hu, J., Du, C., 2013. Why are some marginal seas sources of atmospheric CO_2? Geophys. Res. Lett. 40, 2154–2158.

Dai, M.H., Gan, J.P., Han, A.Q., Kung, H.S., Yin, Z.Q., 2014. Physical dynamics and biogeochemistry of the Pearl River plume. In: Bianchi, T., Allison, M., Cai, W.-J. (Eds.), Biogeochemical Dynamics at Major River-Coastal Interfaces-Linkages with Global Change. Cambridge University Press, New York, pp. 321–352.

Dippner, J.W., Nguyen, K.V., Hein, H., Ohde, T., Loick, N., 2007. Monsoon-induced upwelling off the Vietnamese coast. Ocean Dyn. 57 (1), 46–62.

Fassbender, A.J., Rodgers, K.B., Palevsky, H.I., Sabine, C.L., 2018. Seasonal asymmetry in the evolution of surface ocean pCO_2 and pH thermodynamic drivers and the influence on sea-air CO_2 flux. Global Biogeochem. Cycles 32, 1476–1497.

Fransson, A., Chierici, M., Nojiri, Y., 2006. Increased net CO_2 outgassing in the upwelling region of the southern Bering Sea in a period of variable marine climate between 1995 and 2001. J. Geophys. Res.-Oceans 111, C08008 doi:08010.01029/02004JC002759.

Friederich, G.E., Ledesma, J., Ulloa, O., Chavez, F.P., 2008. Air-sea carbon dioxide fluxes in the coastal southeastern tropical Pacific. Prog. Oceanogr. 79 (2–4), 156–166.

Friederich, G.E., Walz, P.M., Burczynski, M.G., Chavez, F.P., 2002. Inorganic carbon in the central California upwelling system during the 1997–1999 El Nino-La Nina event. Prog. Oceanogr. 54 (1–4), 185–203.

Gan, J.P., Li, L., Wang, D.X., Guo, X.G., 2009. Interaction of a river plume with coastal upwelling in the northeastern South China Sea. Cont. Shelf Res. 29 (4), 728–740.

Guan, H., Wang, H.-J., Zhou, L., Yang, S., 2011. A numerical simulation study on the typhoon-ocean interaction in the South China Sea. Chin. J. Geophys. 54 (5), 1141–1149 (in Chinese with English abstrat).

Guo, X.H., Zhai, W.D., Dai, M.H., Zhang, C., Bai, Y., Xu, Y., Li, Q., Wang, G.Z., 2015. Air-sea CO_2 fluxes in the East China Sea based on multiple-year underway observations. Biogeosciences 12 (18), 5495–5514.

Hales, B., Takahashi, T., Bandstra, L., 2005. Atmospheric CO_2 uptake by a coastal upwelling system. Global Biogeochem. Cycles 19 (1), GB1009 doi:1010.1029/2004GB002295.

Hu, J., Kawamura, H., Hong, H., Qi, Y., 2000. A review on the currents in the South China Sea: Seasonal circulation, South China Sea Current and Kuroshio intrusion. J. Oceanogr. 56, 607–624.

Huang, W.-J., Cai, W.-J., Wang, Y., Lohrenz, S.E., Murrell, M.C., 2015. The carbon dioxide system on the Mississippi River -dominated continental shelf in the northern Gulf of Mexico: 1. Distribution and air-sea CO_2 flux. J. Geophys. Res.-Oceans 120 (3), 1429–1445.

Jiang, L.Q., Cai, W.-J., Wanninkhof, R., Wang, Y.C., Luger, H., 2008. Air-sea CO_2 fluxes on the US South Atlantic Bight: Spatial and seasonal variability. J. Geophys. Res.-Oceans 113, C07019 doi:07010.01029/02007JC004366.

Laruelle, G.G., Cai, W.-J., Hu, X., Gruber, N., Mackenzie, F.T., Regnier, P., 2018. Continental shelves as a variable but increasing global sink for atmospheric carbon dioxide. Nat. Commun. 9, 454 doi:410.1038/s41467-41017-02738-z.

Laruelle, G.G., Durr, H.H., Slomp, C.P., Borges, A.V., 2010. Evaluation of sinks and sources of CO_2 in the global coastal ocean using a spatially-explicit typology of estuaries and continental shelves. Geophys. Res. Lett. 37, L15607 doi:15610.11029/12010GL043691.

Laruelle, G.G., Lauerwald, R., Pfeil, B., Regnier, P., 2014. Regionalized global budget of the CO_2 exchange at the air-water interface in continental shelf seas. Global Biogeochem. Cycles 28 (11), 1199–1214.

Liu, Q.Y., Kaneko, A., Su, J.L., 2008. Recent progress in studies of the South China Sea circulation. J. Oceanogr. 64 (5), 753–762.

Lv, Y., Bai, Y., Li, Q., Jiang, H., 2018. Satellite remote sensing retrieval of aquatic pCO_2 in

summer in the Pearl River estuary. J. Marine Sci. 36 (2), 1–11 (in Chinese with English abstract).
Ma, Y., Gao, Q., Li, T., Cai, Y., Zhang, Q., Shi, H., Zhang, J., Wang, D., 2016. The changes of partial pressure of carbon dioxide in surface water in the northwen South China Sea under the influence of El Nino in spring. Acta Scientiae Circumstantiae 36 (10), 2581–2588 (in Chinse with English abstract).
Marrec, P., Cariou, T., Mace, E., Morin, P., Salt, L.A., Vernet, M., Taylor, B., Paxman, K., Bozec, Y., 2015. Dynamics of air-sea CO_2 fluxes in the northwestern European shelf based on voluntary observing ship and satellite observations. Biogeosciences 12 (18), 5371–5391.
McKee, B.A., Aller, R.C., Allison, M.A., Bianchi, T.S., Kineke, G.C., 2004. Transport and transformation of dissolved and particulate materials on continental margins influenced by major rivers: benthic boundary layer and seabed processes. Cont. Shelf Res. 24 (7–8), 899–926.
Pierrot, D., Neill, C., Sullivan, K., Castle, R., Wanninkhof, R., Luger, H., Johannessen, T., Olsen, A., Feely, R.A., Cosca, C.E., 2009. Recommendations for autonomous underway pCO_2 measuring systems and data-reduction routines. Deep-Sea Res. II 56 (8–10), 512–522.
Rehder, G., Suess, E., 2001. Methane and pCO_2 in the Kuroshio and the South China Sea during maximum summer surface temperatures. Mar. Chem. 75 (1–2), 89–108.
Salt, L.A., Thomas, H., Prowe, A.E.F., Borges, A.V., Bozec, Y., de Baar, H.J.W., 2013. Variability of North Sea pH and CO_2 in response to North Atlantic Oscillation forcing. J. Geophys. Res.-Biogeosci. 118, 1584–1592.
Sarma, V., Kumar, M.D., George, M.D., 1998. The central and eastern Arabian Sea as a perennial source of atmospheric carbon dioxide. Tellus B 50 (2), 179–184.
Sarma, V., Swathi, P.S., Kumar, M.D., Prasannakumar, S., Bhattathiri, P.M.A., Madhupratap, M., Ramaswamy, V., Sarin, M.M., Gauns, M., Ramaiah, N., Sardessai, S., de Sousa, S.N., 2003. Carbon budget in the eastern and central Arabian Sea: an Indian JGOFS synthesis. Global Biogeochem. Cycles 17 (4), 1102 doi:1110.1029/2002GB001978.
Sheu, D.D., Chou, W.C., Wei, C.L., Hou, W.P., Wong, G.T.F., Hsu, C.W., 2010. Influence of El Nino the sea-to-air CO_2 flux at the SEATS time-series site, northern South China Sea. J. Geophys. Res.-Oceans 115, C10021 doi:10010.11029/12009JC006013.
Stoll, M.H.C., Thomas, H., De Baar, H.J.W., Zondervan, I., De Jong, E., Bathmann, U.V., Fahrbach, E., 2002. Biological versus physical processes as drivers of large oscillations of the air-sea CO_2 flux in the Antarctic marginal ice zone during summer. Deep-Sea Research I 49 (9), 1651–1667.
Su, J.L., 2004. Overview of the South China Sea circulation and its influence on the coastal physical oceanography outside the Pearl River Estuary. Cont. Shelf Res. 24 (16), 1745–1760.
Sweeney, C., Gloor, E., Jacobson, A.R., Key, R.M., McKinley, G., Sarmiento, J.L., Wanninkhof, R., 2007. Constraining global air-sea gas exchange for CO_2 with recent bomb C-14 measurements. Global Biogeochem. Cycles 21 (2), GB2015 doi:2010.1029/2006GB002784.
Takahashi, T., Olafsson, J., Goddard, J.G., Chipman, D.W., Sutherland, S.C., 1993. Seasonal variation of CO_2 and nutrients in the high latitude surface oceans-a comparative study. Global Biogeochem. Cycles 7 (4), 843–878.
Takahashi, T., Sutherland, S.C., Wanninkhof, R., Sweeney, C., Feely, R.A., Chipman, D.W., Hales, B., Friederich, G., Chavez, F., Sabine, C., Watson, A., Bakker, D.C.E., Schuster, U., Metzl, N., Yoshikawa-Inoue, H., Ishii, M., Midorikawa, T., Nojiri, Y., Kortzinger, A., Steinhoff, T., Hoppema, M., Olafsson, J., Arnarson, T.S., Tilbrook, B., Johannessen, T., Olsen, A., Bellerby, R., Wong, C.S., Delille, B., Bates, N.R., de Baar, H.J.W., 2009. Climatological mean and decadal change in surface ocean pCO_2, and net sea-air CO_2 flux over the global oceans. Deep-Sea Res. II 56 (8–10), 554–577.
Tan, S.C., Shi, G.Y., 2009. Spatiotemporal variability of satellite-derived primary production in the South China Sea, 1998–2006. J. Geophys. Res.-Biogeosci. 114, G03015 doi:03010.01029/02008JG000854.
Tang, L., Zhan, J.-M., Chen, Y.-Z., Li, Y.-S., Nie, Y.-H., 2011. Typhoon process and its impact on the surface circulation in the northern South China Sea. J. Hydrodynamics 23 (1), 95–104.
Thomas, H., Schneider, B., 1999. The seasonal cycle of carbon dioxide in Baltic Sea surface waters. J. Mar. Syst. 22 (1), 53–67.
Torres, R., Pantoja, S., Harada, N., Gonzalez, H.E., Daneri, G., Frangopulos, M., Rutllant, J.A., Duarte, C.M., Ruiz-Halpern, S., Mayol, E., Fukasawa, M., 2011. Air-sea CO_2 fluxes along the coast of Chile: From CO_2 outgassing in central northern upwelling waters to CO_2 uptake in southern Patagonian fjords. J. Geophys. Res.-Oceans 116, C09006 doi:09010.01029/02010JC006344.
Torres, R., Turner, D.R., Rutllant, J., Lefevre, N., 2003. Continued CO_2 outgassing in an upwelling area off northern Chile during the development phase of El Nino 1997–1998 (July 1997). J. Geophys. Res.-Oceans 108, 3336 doi:3310.1029/2000JC000569.
Tseng, C.M., Wong, G.T.F., Chou, W.C., Lee, B.S., Sheu, D.D., Liu, K.K., 2007. Temporal variations in the carbonate system in the upper layer at the SEATS station. Deep-Sea Res. II 54, 1448–1468.
Wang, G., Dai, M., Shen, S.S.P., Bai, Y., Xu, Y., 2014. Quantifying uncertainty sources in the gridded data of sea surface CO_2 partial pressure. J. Geophys. Res.-Oceans 119 (8), 5181–5189.
Wang, G.H., Su, J.L., Chu, P.C., 2003. Mesoscale eddies in the South China Sea observed with altimeter data. Geophys. Res. Lett. 30 (21), 2121 doi:2110.1029/2003GL018532.
Wang, Z.H.A., Wanninkhof, R., Cai, W.-J., Byrne, R.H., Hu, X.P., Peng, T.H., Huang, W.J., 2013. The marine inorganic carbon system along the Gulf of Mexico and Atlantic coasts of the United States: insights from a transregional coastal carbon study. Limnol. Oceanogr. 58 (1), 325–342.
Wanninkhof, R., 1992. Relationship between wind speed and gas exchange over the ocean. J. Geophys. Res.-Oceans 97 (C05), 7373–7382.
Wanninkhof, R., Asher, W.E., Ho, D.T., Sweeney, C., McGillis, W.R., 2009. Advances in quantifying air-sea gas exchange and environmental forcing. Annu. Rev. Marine Sci. 1, 213–244.
Wanninkhof, R., Doney, S.C., Takahashi, T., McGillis, W., 2002. The effect of using time-averaged winds on regional air-sea CO_2 fluxes, Gas Transfer at Water Surfaces. In: Geophys. Monogr. Ser. 127. DonelanAmrican Geophysical Union, Washington, D.C, pp. 351–357.
Weiss, R.F., 1974. Carbon dioxide in water and seawater: the solubility of a non-ideal gas. Mar. Chem. 2, 203–215.
Weiss, R.F., Price, B.A., 1980. Nitrous oxide solubility in water and seawater. Mar. Chem. 8 (4), 347–359.
Wesslander, K., Omstedt, A., Schneider, B., 2010. Inter-annual and seasonal variations in the air-sea CO_2 balance in the central Baltic Sea and the Kattegat. Cont. Shelf Res. 30 (14), 1511–1521.
Woosley, R.L., 2018. Complexity of marine CO_2 system highlighted by seasonal asymmetries. Global Biogeochem. Cycles 32, 1434–1436.
Xu, X., Yu, P., Cai, X., Pan, J., Hu, J., Zhang, H., 2016. Distributions of partial pressure of carbon dioxide and sea-air CO_2 flux in the western South China Sea in autumn. J. Tropical Oceanogr. 35 (3), 55–64 (in Chinese with English abstract).
Zhai, W., 2015. Sea surface partial pressure of CO_2 and its controls in the northern South China Sea in the non-bloom period in spring. Haiyang Xuebao 37 (6), 31–37 (in Chinese with English abstract).
Zhai, W., Dai, M., Chen, B., Guo, X., Li, Q., Shang, S., Zhang, C., Cai, W.-J., Wang, D., 2013. Seasonal variations of sea-air CO_2 fluxes in the largest tropical marginal sea (South China Sea) based on multiple-year underway measurements. Biogeosciences 10, 7775–7791.
Zhai, W.D., Dai, M.H., Cai, W.-J., 2009. Coupling of surface pCO_2 and dissolved oxygen in the northern South China Sea: impacts of contrasting coastal processes. Biogeosciences 6 (11), 2589–2598.
Zhai, W.D., Dai, M.H., Cai, W.-J., Wang, Y.C., Hong, H.S., 2005. The partial pressure of carbon dioxide and air-sea fluxes in the northern South China Sea in spring, summer and autumn. Mar. Chem. 96 (1–2), 87–97.
Zhou, K., Dai, M., Kao, S.-J., Wang, L., Xiu, P., Chai, F., Tian, J., Liu, Y., 2013. Apparent enhancement of ^{234}Th-based particle export associated with anticyclonic eddies. Earth Planet. Sci. Lett. 381, 198–209.